Advanced Injectors for Chemical Rockets Inspired by Ink-jet Printing Technology

Final Report

Authors: Dr Peter Glynne-Jones[1], Michele Coletti[2], Prof Steven Gabriel[2], Prof. Neil White[1], Dr Steve Beeby[1]

Affiliation: (1) School of Electronics and Computer Science, University of Southampton.
(2) School of Engineering Science, University of Southampton, UK

ESA Researcher(s): Cristina Bramanti

Contacts:
Steven Gabriel
Tel: +44(0)2380 593222
e-mail: sbg2@soton.ac.uk

Cristina Bramanti
Tel: +31(0)71 565 8882
Fax: +31(0)71 565 8018
e-mail: act@esa.int

Available on the ACT website
http://www.esa.int/act

Ariadna ID: 06/3101
Study Duration: 4 months
Contract Number: 20275/06/NL/HE

Abstract

Control over drop size distributions, injection rates, and geometrical distribution of fuel and oxidiser sprays in bi-propellant rocket engines has the potential to produce more efficient, more stable, less polluting rocket engines. This control also offers the potential of an engine that can be throttled, working efficiently over a wide range of output thrusts. Inkjet printing technologies, MEMS fuel atomisers, piezoelectric injectors for diesel engines, and electrospray injectors are considered for their potential to yield a new, more active injection scheme for a rocket engine. Inkjets are found to be unable to pump at sufficient pressures, and have possibly dangerous failure modes. Active injection is found to be feasible if high pressure drop along the injector plate are used. A conceptual design is presented and its basic behaviour assessed. The possibility of using an array of electrospray injectors has been evaluated finding good performances with acceptable power requirements.

Contents

1 List of Figures and Tables....2
2 Abbreviations....3
3 Introduction....3
4 Inkjets....5
4.1 Surface Tension....10
4.2 Fundamental Inkjet limits....11
4.2.1 Push-mode actuation....11
4.2.2 Bend-mode actuation....13
4.2.3 Determining Pump characteristics....14
4.3 Inkjet characteristics required for a rocket engine....15
5 Excitation for Enhanced Atomisation....18
5.1 A MEMS fuel pump / atomiser – Nabity et al....18
5.2 Assessing excitation for enhanced atomisation....20
5.3 Other methods of enhancing atomisation....25
6 Electrospray injectors [37,38]....27
7 Diesel injectors....29
7.1 Introduction....29
7.2 Droplet size....32
7.3 Applicability to rockets....33
7.4 Fuel Injector Conclusions....37
7.5 Active injection – a design concept....38
8 Pump and Nozzle Materials and manufacture....41
9 Conclusions and Recommendations....44
10 Acknowledgements....45
11 References....45
Appendix A: Micropump data....49

1 List of Figures and Tables

Figure 1 Continuous Inkjet, a binary deflection system (from Le Hue[1]) 5
Figure 2 Thermal inkjet (from Le Hue [1]) 6
Figure 3 Electrostatic Inkjet design (from Kamisuki [3]) 7
Figure 4 Piezoelectric inkjet configurations (from Le Hue [1]) 8
Figure 5 Shear-mode inkjet (from Brunahl [5]) 9
Figure 6 Deformed finite-element model of shear-mode inkjet actuator wall. Colours show the potential distribution resulting from 18V applied voltage. 9
Figure 7 Graph showing pressure required to overcome surface tension at various nozzle sizes 10
Figure 8 push mode actuator 11
Figure 9 Typical micropump characteristics 12
Figure 10 Membrane actuator, from Morgan [10] 13
Figure 11 Operation of a valveless micropump (from Ahmadian et al [12]) 14
Figure 12 Ideal Inkjet characteristics 15
Figure 13 Rocket requirements compared to ideal and actual inkjet performance 17
Figure 14 A MEMS Fuel atomiser (from Nabity et al [15]) 19
Figure 15 – MEMS atomizer schematic 20
Figure 16 – Grow factor for a MMH and NTO 23
Figure 17 pressure trend with time at the exit of the injector, f_{MMH} = 16500 Hz f_{NTO} 9700 Hz 24
Figure 18 velocity trend with time at the exit of the injector, f_{MMH} = 16500 Hz f_{NTO} 9700 Hz 24
Figure 19 velocity and pressure trend with frequency at the exit of the injector 25
Figure 20 Diagrams from US Patent 5,873,240: Pulsed Detonation Rocket Engine. 27
Figure 21 – MEMS array of elecrospray nozzles [37] 27
Figure 22 multiplexed electrospray configuration used by Deng et al. [37,39,40] 28
Figure 23 In-line diesel injection (from [20]) 29
Figure 24 Common Rail Fuel injector (from Bosch [21], pp. 310) 31
Figure 25 Injector nozzles (from Bae [23]) 32
Figure 26 Effects of injection pressure and time on SMD of the spray from VCO nozzle (0.144mm x 5hole) (from Bae [23]) 32
Figure 27 Mechanical jet break-up regimes (from Faeth [26]) 34
Figure 28 – Break-up modes for different pressures and pressures drops D=100μm 36
Figure 29 - Break-up modes for different pressures and pressures drops D=50μm 36
Figure 30 - Break-up modes for different pressures and pressures drops D=200μm 37
Figure 31 Proposed Active Injector system (not to scale) 39
Figure 32 Tektronix piezoelectric inkjet, stainless steel stack (from Le Hue [1]) 42
Figure 33 An SEM photograph of an EDM stainless steel nozzle (from Le Hue [1]) 43

Table 1 Fuel flow rates required for rocket engines 16
Table 2 MEMS injector design for a 40 N thruster 23
Table 3 Multiplexed electrospray application to a 4N and 40N thruster 28
Table 4 Fuel properties 35
Table 5 Active Injector Design parameters 40

2 Abbreviations

AFM	Abrasive Flow Machining
DOD	Drop on Demand
EDM	Electrical Discharge Machining
MEMS	Micro Electro-Mechanical Systems
MMH	Monomethylhydrazine, $CH_3N_2H_3$
NTO	Nitrogen tetroxide, N_2O_4
PDE	Pulse Detonation Engine
PZT	Lead Zirconium Titanate, a piezoelectric material.
SMD	Sauter Mean Diameter

3 Introduction

The injectors in a chemical rocket motor are key in determining the efficiency of the reactions within the combustion chamber, ultimately affecting the performance of the motor, heat loads, etc. Critical to achieving good performance is the atomisation process, whereby the propellant and oxidiser are transformed into small droplets; in essence the size of these drops determines the mixing process and evaporation rates, which have a profound influence on the combustion reactions.

The basic function of the injector in a bipropellant liquid rocket is to atomise and mix the fuel with the oxidiser to produce efficient and stable combustion that will produce the required thrust without endangering hardware durability. Currently, most bipropellant rockets and hybrid rockets use small orifices in the injector plate, which takes the form of a perforated disk at the head of the combustion chamber. To achieve high combustion performance and stable operation without affecting injector and thrust chamber durability requires proper selection and design specification of the entire flow-system geometry, which consists of the total element pattern, the individual orifice geometry and the flow system upstream of the orifices. The spray distributions (i.e. mass, mixture ratio and drop size distributions) are specified by the design of the complete flow-system geometry.

To arrive at the specification of the mixing and propellant drop size levels in the combustion chamber, combustion models are used and the results of these combustion model programs and experiments, have shown that combustion performance is highly dependent on the propellant spray distributions; high efficiency requires uniform mixture-ratio distribution, initial drop size consistent with the chamber geometry and operating conditions, and a uniform mass distribution.

The local mixture ratio and mass distributions near the injector face or chamber walls and also the radial and transverse flows produced by adverse distributions of the overall mass

or mixture ratio can have a strong impact on hardware durability; high rates of chemical reactions or material erosion caused by impingement of highly reactive propellants on the chamber wall can cause catastrophic damage of the chamber.

Thus more control over drop size distributions, injection rates, and geometrical distribution of fuel and oxidiser sprays has the potential to produce more efficient, more stable, less polluting rocket engines. This control also offers the potential of an engine that can be throttled, working efficiently over a wide range of output thrusts.

Inkjet printing technologies, MEMS fuel atomisers, piezoelectric injectors for diesel engines, and electrospray injectors are considered in the following report for their potential to yield a new, more active injection scheme for a rocket engine.

4 Inkjets

Inkjet technologies can be split into two fundamental types: continuous and drop-on-demand (DOD).

Continuous inkjet designs are used in high volume applications. Figure 1 shows a binary deflection system. The ink is supplied under pressure, and passes through a nozzle. The nozzle is excited at a frequency that promotes break-up of the jet into droplets around twice the size of the nozzle. The remaining parts of the system are used to deflect droplets away from the paper when printing is not required. The possibility of promoting atomisation in a rocket injector in this manner will be considered further below, though it should be noted that much more efficient atomisation is possible: under high pressure or with impinging flows droplets can be much smaller than the nozzle diameter.

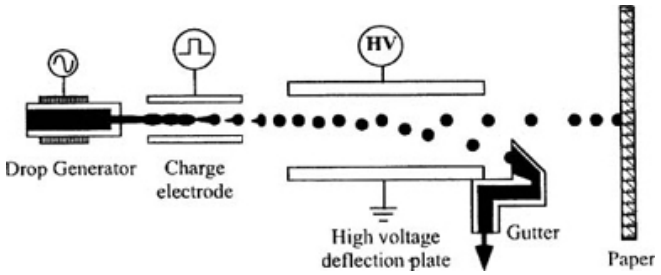

Figure 1 Continuous Inkjet, a binary deflection system (from Le Hue[1])

Drop-on-demand inkjets are used in the majority of printers. There are three major types, based on the form of actuation: thermal, piezoelectric and electrostatic ink-jets. In all three types, ink is supplied at ambient pressure, and is kept from leaving the printer nozzle by surface tension. Thermal inkjets are the most common type used in household printers, followed by piezoelectric ones.

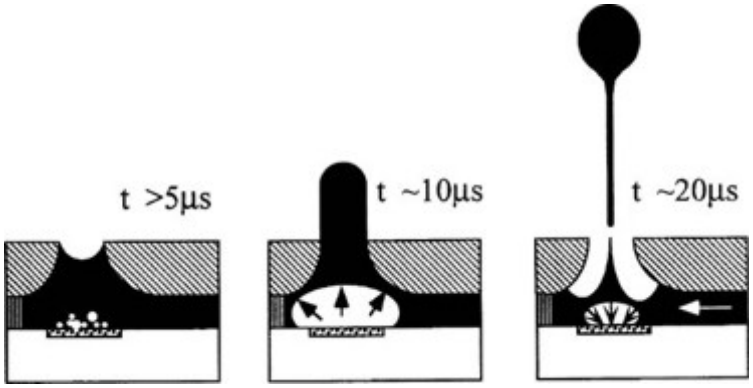

Figure 2 Thermal inkjet (from Le Hue [1])

Figure 2 shows the formation of a droplet in a thermal inkjet printer. In this basic design, the water based ink is superheated by applying a current pulse of a few micro-seconds to an electrical heater located under the nozzle. A bubble forms very rapidly and pushes out a droplet. As the heat in the bubble is exhausted the bubble collapses and more ink is drawn in from the reservoir. The advantage of thermal inkjets is their speed and the ease of miniaturisation, but they consume more power than piezoelectric designs [1]. The current trend in inkjet printers is towards larger arrays of more closely spaced nozzles, and smaller droplet sizes. For example the print-head of the Cannon i950 photo printer which uses their 'MicroFine Droplet Technology™' has 3072 nozzles, each capable of ejecting droplets of volume 2pL (corresponding to a droplet diameter 16µm) at a rate of 24kHz. This represents a maximum flow rate of 0.15ml/sec. Thus it can be seen that to achieve the 12.5ml/sec fuel flow required for a typical 40N thruster we would need over 80 such print-*heads*. The large power consumption of thermal inkjets is the real obstacle to their use as fuel injectors: Chen [2] reports a typical energy of 11.5µJ per droplet (of volume 34pl), which corresponds to a power consumption of over 4000W for the fuel flow required for a 40N thruster: This is clearly impractical, and thermal inkjets will not be considered further.

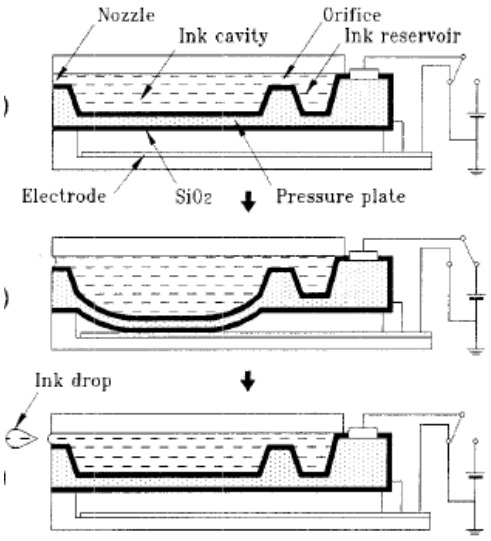

Figure 3 Electrostatic Inkjet design (from Kamisuki [3])

Figure 3 shows and electrostatic inkjet design. Electrostatic inkjet designs are capable of similar volume pumping rates to piezoelectric designs. The maximum pressure that an electrostatically actuated membrane can generate is given by:

$$P = \frac{\varepsilon V^2}{2s^2} \tag{1}$$

where ε is the permittivity of the medium separating the plates, s the distance between the plate, and V is the potential difference between them [4]. For example to produce an initial pressure (driver force per unit diaphragm area) of 1 bar from an electrostatic actuator acting in a vacuum requires a voltage/separation distance ratio of $150 V \mu m^{-1}$. The silicon dioxide layer used to separate the electrodes of electrostatic actuators has dielectric breakdown strength of 800-1000 $V \mu m^{-1}$. Allowing for some additional initial electrode separation, this results in a maximum initial pressure of around 4 bar.

Piezoelectric inkjets can be divided into three main categories according to the piezoelectric actuation mode: push, bend and shear. The first two are illustrated in Figure 4. All rely on the deformation of the piezoelectric element to push out a droplet from the nozzle, and all three types have been used in commercial designs.

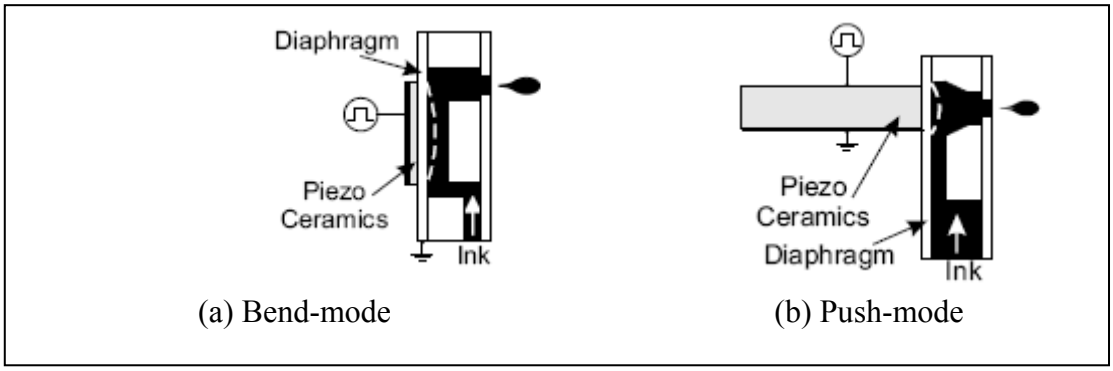

Figure 4 Piezoelectric inkjet configurations (from Le Hue [1])

The push-mode inkjet uses a PZT rod to push out the ink. In practice a thin membrane is placed between the rod and the ink to prevent interaction.

In the bend-mode inkjet a piezoelectric element causes the diaphragm to flex. Typically, a piezoelectric layer is adhered to a thin steel or silicon membrane. When the piezoelectric layer is actuated it expands laterally, and in the manner of a bi-morph the resulting difference in strain between the piezoelectric and membrane causes the membrane to deflect either up or down.

The shear-mode inkjet, shown in Figure 5, has electrodes deposited on the upper half of both sides of the channel walls. The applied field is thus perpendicular to the direction of polarisation, and causes the walls to shear sideways, and squeeze out an ink drop (shearing is one of the modes of displacement of a piezoelectric element). The actuator is manufactured from a solid block of PZT by sawing the grooves, and then depositing electrodes.

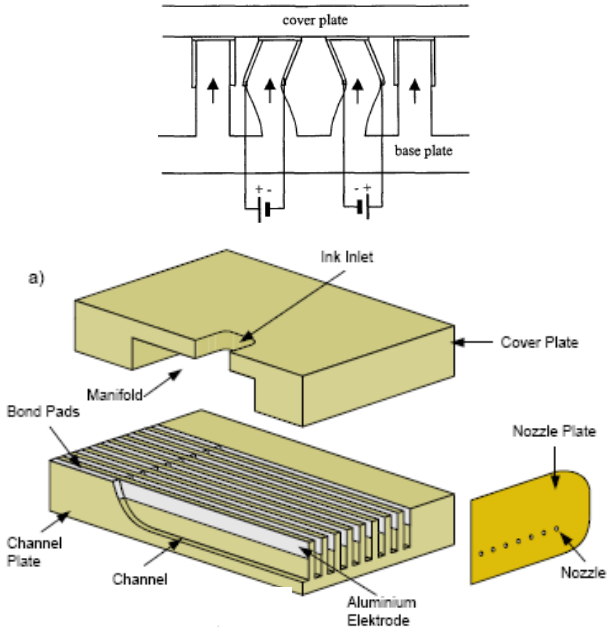

Figure 5 Shear-mode inkjet (from Brunahl [5])

The commercially produced shear-mode inkjet, Xaar's XJ128 produces drops of diameter 42µm at a rate of 8kHz and velocity of 10m/s. This is comparable to typical piezoelectric bend-mode and electrostatic designs. Its power consumption is much higher than a bend-mode design – to pump enough fuel for a 40N thruster (see section 4.3 for details of calculations) would need approximately 330W electrical power; this is impractically large. To investigate the flow pressure (see section 4.2.1) that the inkjet could operate against (blocking pressure), a finite element model was produced using the ANSYS program. Figure 6 shows the deformed shape when 18V are applied across the electrodes. The model produces a deflection close to that observed by Bruhnal [5]. By constraining the sideways deflection and measuring the resulting reaction forces, the blocking pressure of the actuator was found to be 3.6 bar. It will be shown below that this is comparable to a membrane actuated inkjet. The much larger power-consumption rules it out as a practical injector, so only bend-mode and push-mode actuators will be considered in the sections that follow.

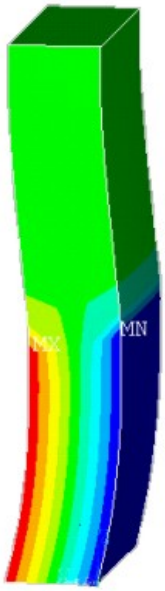

Figure 6 Deformed finite-element model of shear-mode inkjet actuator wall. Colours show the potential distribution resulting from 18V applied voltage.

4.1 Surface Tension

In inkjet printers surface tension prevents unwanted ink flow out of the nozzle, and also prevents net backflow. The ink reservoir of an inkjet printer is not pressurised, and the question here is whether the surface tension will be sufficient to prevent flow when used in conjunction with a combustion chamber and pressurised fuel tank.

It should also be noted that the meniscus of an inkjet usually retracts some distance (e.g. 3 nozzle diameters [6]) into the chamber of the inkjet. If in a rocket engine this drew some combusting gases into the inkjet, there is a danger of damage to the inkjet.

The pressure difference required to overcome surface tension is given [7] by:

$$\Delta P = \frac{4\sigma}{d} \tag{2}$$

Where σ is the coefficient of surface tension and d the diameter of the nozzle. Figure 7 shows the pressure required to push droplets of MMH and NTO fuels through a variety of nozzle sizes as calculated by the equation. It can be seen that at typical nozzle sizes of 20µm or more any pressure difference above about 0.06 bar would cause fuel to flow in or out of the nozzle.

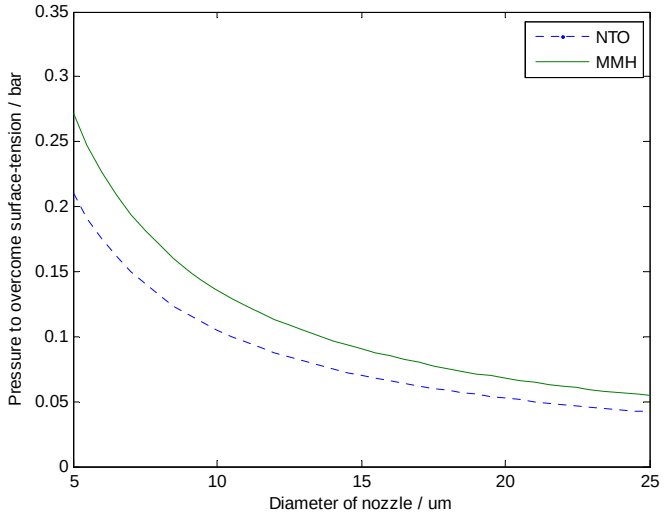

Figure 7 Graph showing pressure required to overcome surface tension at various nozzle sizes

This has several consequences:

(a) If fuel pressure was greater than the chamber pressure, as in a conventional rocket engine, then fuel would flow whether the inkjet was actuated or not, and only a jet of fuel would emerge from the nozzle rather than droplets. This defeats the point of having an inkjet.

(b) If fuel pressure was lower than chamber pressure, then to prevent backflow valves would be needed to isolate any injectors that were not being actuated. This adds a degree of complexity to an inkjet injector design, but is feasible as integrated micro-valves are a promising area of study for several research groups [8]. The failure of such valves could be catastrophic, with combustion products entering the fuel lines. It will be shown below, however, that inkjets are not capable of supplying sufficient pressure to operate in this configuration.

(c) Trying to match fuel pressure to combustion chamber pressure would be a complex way to ease these problems. If the chamber pressure were constant then inkjets would be able to supply sufficient flow rate (see below). However, fluctuations in chamber pressure are allowed for in conventional designs. If the magnitude of these fluctuation were bigger than the surface tension then either case a) or b) would happen. In the section that follows we will asses what level of fluctuations a piezoelectric actuator could accommodate.

4.2 Fundamental Inkjet limits

The physics of how inkjets are actuated places some upper limits on their flow rate and maximum back-pressure.

4.2.1 Push-mode actuation

Figure 8 shows a cylindrical piezoelectric cylinder. When a voltage is applied to the actuator there will be a displacement. When this displacement is blocked, a force will develop, the so-called blocking force [10].

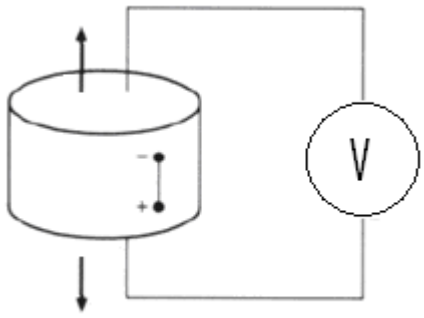

Figure 8 push mode actuator

The relationship of volume displacement to pressure applied is shown in Figure 9, and it shows that the maximum displacement is only achieved if there is no pressure applied to

the actuator face. If the actuator is to be used in a pump, the blocking pressure must be much larger than the pressure difference that the pump is required to work against; otherwise there will be a corresponding decrease in the pumped volume.

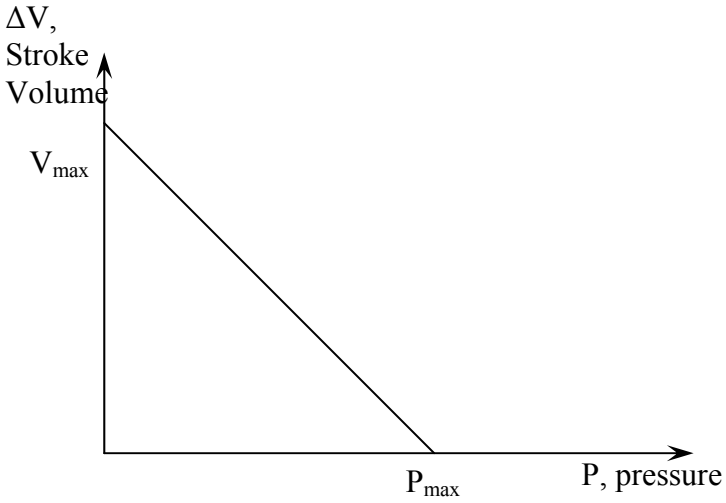

Figure 9 Typical micropump characteristics

The stroke volume, ΔV_{MAX}, of a piezoelectric cylinder expanding along its axis is given by [10]:

$$\Delta V_{MAX} = d_{33} AhE \tag{3}$$

Where d_{33} is a piezoelectric coefficient, A the area of the top face, and E the applied electric field.

The blocking pressure, P_{max}, is given by

$$P_{\max} = \frac{d_{33}E}{s_{33}} \tag{4}$$

where s_{33} is the compliance of the piezoelectric disc, and h its thickness. It should be noted that the stroke volume is proportional to the volume of the actuator, and that neither it, nor the blocking pressure are affected by the geometry of the actuator.

Morgan Matroc [10] gives the example of a PXE 5 cylinder 20mm in diameter and 1mm thick, to which a 300V voltage is applied. This results in a blocking pressure of 65 bar and volume displacement of 36.75 x 10^{-3} mm^3.

The power consumption of a push-mode actuator is much high than that of a bend-mode one (described next). The power consumption can be approximated as

$$P = f\frac{1}{2}CV^2 \tag{5}$$

where f is the frequency of actuation, C the capacitance of the actuator, and V the applied voltage.

To produce flow sufficient for a typical 40N thruster (see section 4.3 for calculations of flow rate requirements) would require an array of injectors that would consume approximately 80W. Compared this to 5.5W for a bend-mode actuator (see next section) of thickness 0.5mm, diameter 5mm, voltage 150V, blocking pressure 6 bar.

4.2.2 Bend-mode actuation

Bend-mode or membrane actuators produce a higher stroke volume. The membrane effectively amplifies the small lateral movements of the piezoelectric element into a much larger deflection of the membrane.

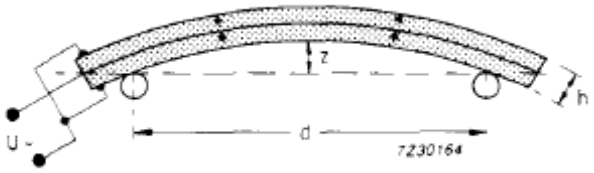

Figure 10 Membrane actuator, from Morgan [10]

The stroke volume versus pressure graph is still of the form shown in Figure 9. For the case of a circular membrane composed of two PZT 5A piezoelectric elements (a bi-morph), the stroke volume can be approximated as: [10],

$$\Delta V = 4 \times 10^{-11} \frac{d^4}{h^2} U \qquad [m^3] \tag{6}$$

where d is the diameter of the membrane, and h the total thickness (in metres). The blocking pressure is:

$$P_{\max} \approx 8 \frac{h}{d^3} U \qquad [Pa] \tag{7}$$

For example: a PZT 5A bimorph of total thickness 0.6mm, and diameter 25mm, actuated at a voltage of 150V gives a stroke volume of 6.5 mm^3 and a blocking pressure of 0.5 bar. We have traded-off pumping pressure for stroke volume.

4.2.3 Determining Pump characteristics

For a given actuator stroke volume and blocking pressure, we wish to determine the characteristics of an inkjet using this element. An important feature of an inkjet, in contrast with many (but not all) micropumps, is that it has no check valves. The mode of operation is shown in Figure 11. During each half of the pumping cycle fluid flows through both the inlet and outlet ports. There is a small directional dependence of the fluidic resistance of the inlet and outlet nozzles (a result of flow separation), which means that overall there is a net pumping action. A more detailed description can be found in Olsson [11].

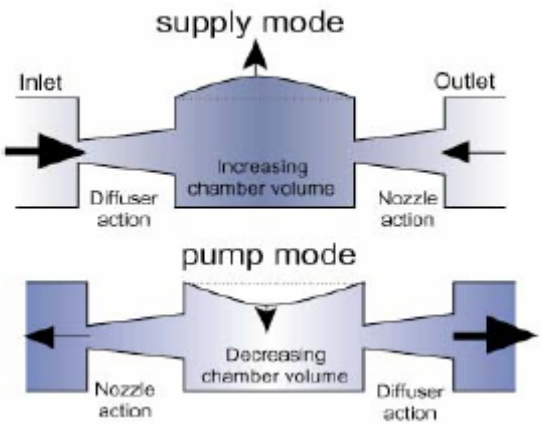

Figure 11 Operation of a valveless micropump (from Ahmadian et al [12])

The ratio of flow rate through the nozzle to flow rate through the diffuser in each mode is typically of the order 4 : 3 [13], and often much less [14]. Thus the maximum droplet volume of an inkjet will be modelled here as one quarter of the displacement volume of the actuator. Similarly the blocking pressure of the pump (the pressure that applied between outlet and inlet will reduce the net flow to zero) will be approximated as one quarter of the blocking pressure of the actuator [14].

The modelling of Nabity [15] described in section 5 explicitly states that they have modelled the inlet and outlet elements as a perfect fluidic diode, which lead one to question the accuracy of their predicted results given this 4 : 3 ratio.

Figure 12 plots the characteristics of inkjets that could be produced from both push-mode and membrane actuators. The y-axis shows the maximum flow-rate divided by total device volume (units min-1). This is sometimes called the self-pumping rate, and a value of, say, 10.0 on this axis would show that an inkjet could pump 10 times its own volume of liquid in each minute. The maximum flow rates have been calculated using an actuation frequency of 10kHz – pumping above this frequency is rarely possible due to inertial effects.

The push-mode acutator is plotted as a point, since its characteristics are determined solely by material properties (PZT-5A is used here). The device volume for the push mode inkjet has been assumed equal to the actuator volume. To calculate the device volume for the membrane inkjet a device height of 2mm for the chamber walls plus the thickness of the membrane has been assumed. A maximum field strength of 300V/m has been used [10].

Each point on the graph corresponds to a particular membrane thickness and diameter. It can be seen that there is an optimum membrane thickness of around 1mm, and that by varying its diameter, a range of different volume / pressure combinations can be obtained. The lines are only plotted for reasonable thickness to diameter ratios of 0.1 or less. Membranes thicker than this would cease to conform to the approximations given above, and perform less well than the approximations might suggest.

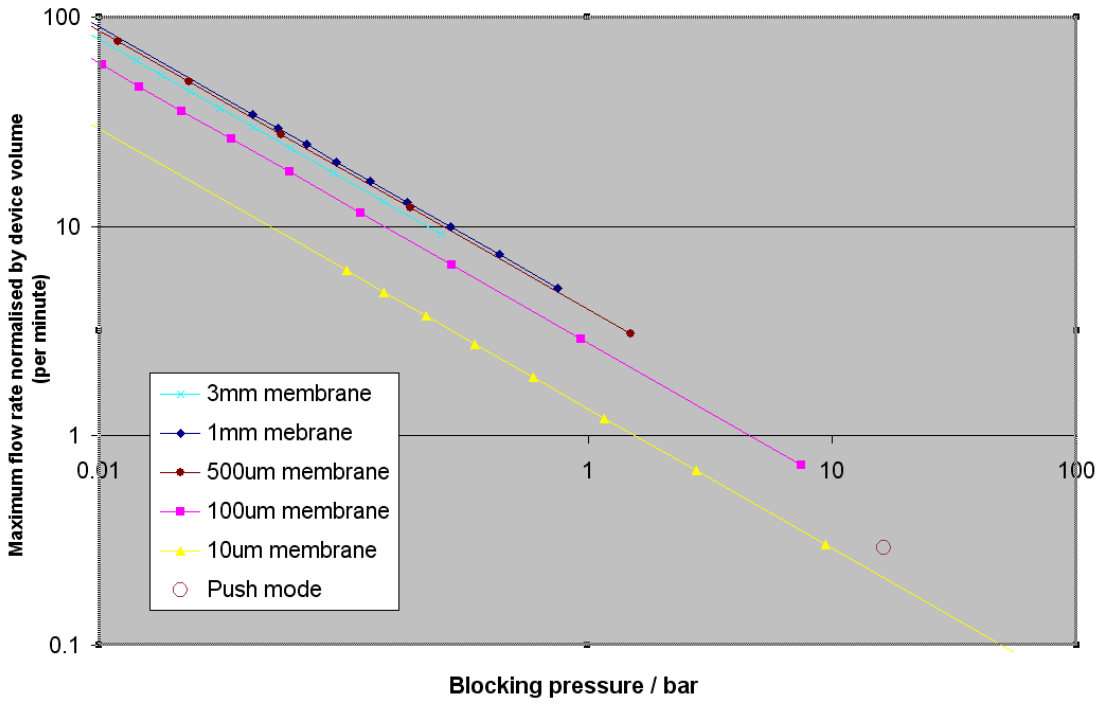

Figure 12 Ideal Inkjet characteristics

4.3 Inkjet characteristics required for a rocket engine

Next to determine what flow rates and maximum pressures an inkjet needs in order to inject fuel into a rocket engine. The estimates in this section are quite loose, but it will be

seen that even if they varied by an order of magnitude the resulting evaluation of feasibility will be unchanged.

The total mass flow rates can be calculated as

$$\dot{m} = \frac{T}{g.I_{sp}} \tag{8}$$

Where g is the gravity acceleration at sea level (9.81 m/s^2), T the thrust, and I_{SP} the specific impulse. For a bipropellant MMH / NTO system I_{SP} is approximately 300s. Table 1 lists the results for a range of thrusts. It also shows the self-pumping rate (flow normalised by total inkjet volume) required given a certain acceptable total inkjet volume. This figure allows us to evaluate whether inkjets can pump suitable volumes of fuel without worrying about how many devices are required. Note that the acceptable volumes have been chosen to given the same normalised flow rate for each example – this makes comparison simpler.

The estimated maximum volumes take no account of the space required for plumbing to supply fuel to each inkjet or how to direct the output into a combustion chamber. The figures given are meant to form a reasonable upper bound.

Engine Thrust	4N	40N	400N
υ, Total Fuel flow (cm^3/min)	75	750	7500
V, Estimated maximum practical volume (cm^3)	1.9 x 1.9 x 1.9	4 x 4 x 4	8.6 x 8.6 x 8.6
Normalised flow rate $\frac{\nu}{V}$ (min^{-1})	11.1	11.1	11.1

Table 1 Fuel flow rates required for rocket engines

To find the minimum blocking pressure that an inkjet would be required to operate at, we consider a system where the fuel pressure is maintained close to the combustion chamber pressure (see section 4.1 above). Existing designs make allowance for pressure fluctuations in the chamber of the order of 10%, e.g. 0.8 bar for an EADS 22N bipropellant thruster [9]. In order that the flow rate is not significantly reduced by the back pressure (and also so that

pressure fluctuations do not cause feedback and instabilities) we propose a blocking pressure of 8 bar. This pressure rules out the use of electrostatic inkjet designs in this case (see the beginning of this section).

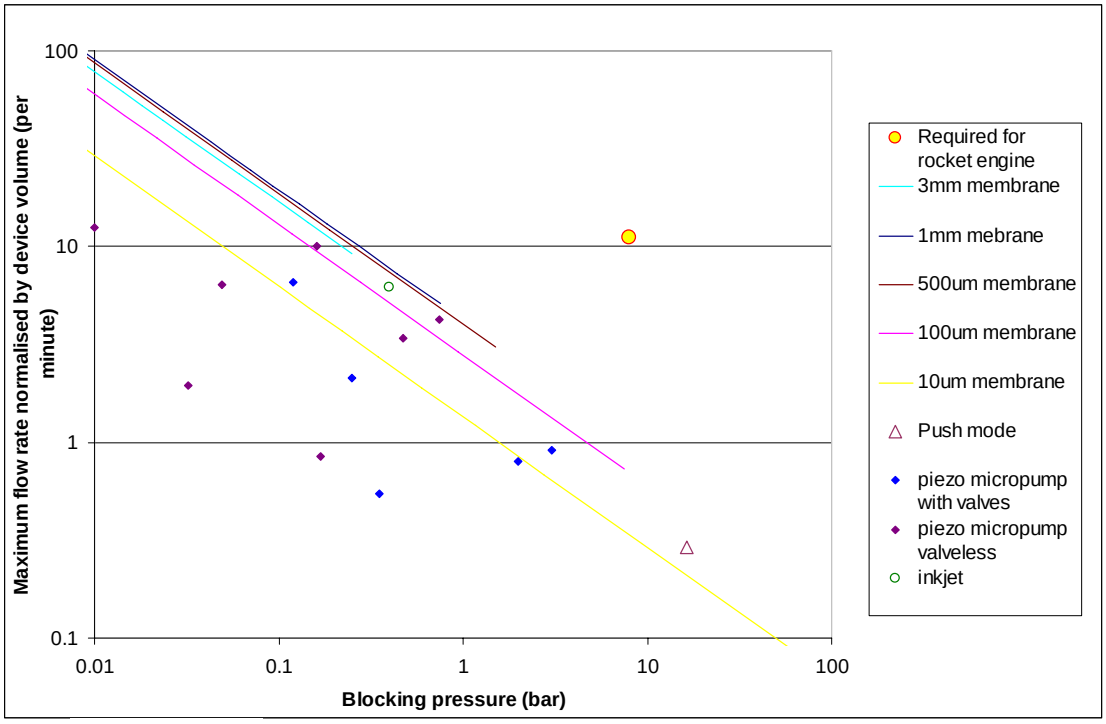

Figure 13 Rocket requirements compared to ideal and actual inkjet performance

Figure 13 plots the required blocking pressure and normalised flow rates, comparing it with the predicted limits of inkjets calculated above. The graph also shows data from a selection of micropumps described in the literature, and includes data for a range of actuator types, including some devices with valves (the raw data for these points is listed in the table in Appendix A). There is only a single point for a real example of an inkjet as the blocking pressure of an inkjet is rarely measured.

It can be seen that although some pump designs can produce sufficient flow, the blocking pressure at these flow rates is more than an order of magnitude below that required.

Thus, even if significant effort were put into developing a high pressure inkjet or micropump, it is unlikely that a design with sufficient flow rate could be produced. And so we conclude that inkjets are not suitable for use as rocket fuel injectors where significant pressure fluctuations exist in the combustion chamber. There is a possibility that the reduced droplet sizes and an active control system might reduce the pressure fluctuations. Inkjets can supply sufficient flow rates, and we estimate that if the pressure fluctuations could be reduced

to less than 0.05 bar (that is 0.6% of a typical 8 bar chamber pressure), then inkjets could supply the required fuel. This may well be unrealisable.

Advances in materials technology would improve the blocking pressure of an inkjet injector. In order to produce a practical injector we estimate that an increase of around 800% in the d_{33} value would be required. The authors are not aware of any material systems that could produce such improvements.

The arguments presented above are also valid for micropumps, except that designs with valves would not suffer the pressure and volume loss caused by not having them; this would be offset however by a much reduced pumping frequency, so micropumps would also be unsuitable in this application. Micropumps with check-valves also (e.g. Li et al in Nyugen [16]) devote considerable space to the valves, increasing the pump volume. Micro-fabricated check-valves are also prone to clogging and can exhibit significant pressure losses [13], and Gravesen [17] notes, "long-term problems related to sedimentation or wear must be foreseen."

5 Excitation for Enhanced Atomisation

5.1 A MEMS fuel pump / atomiser – Nabity et al

This section describes and assesses research carried out in collaboration between TDA Research and the University of Colorado [15], [18]. The research was aimed at producing a MEMS fuel atomiser / pump suitable for use in high performance aircraft and weapons engines. In particular there was concern to produce the very small droplets required to fuel a pulse detonation engine (PDE).

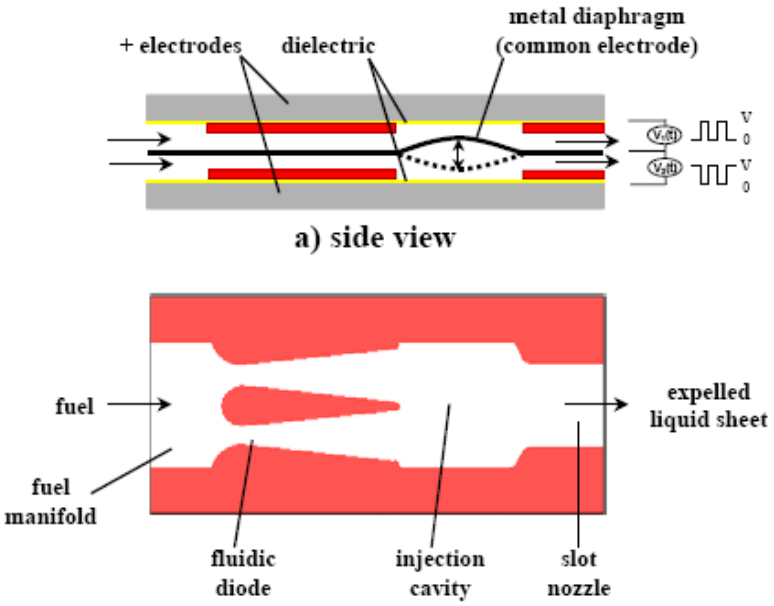

Figure 14 A MEMS Fuel atomiser (from Nabity et al [15])

The papers produced by Nabity et al use the same picture (Figure 14) to describe two distinct devices: (a) The initial paper [15] describes the modelling of a self-aspirating pump; (b) An atomiser [18] - the device is fed pressurised fuel and uses the membrane to excite atomisation of the resulting jet.

(a) As a self-aspirating pump

In this mode, the movement of the electrostatically actuated membrane is used to propel fuel through an array of micro-machined nozzles. This is a valve-less micropump of the sort described in section 4.2.3.

It was not clear from the literature, but on contacting the authors by email, it was confirmed that the device has not been tested in the self-aspirating mode. The flow rate predicted by their modelling needs to be considered carefully – an assumption is made that the inlet and outlet ports act as perfect valves; in such pumps losses usually reduce the volume flow rate by a factor of about 4 [14]. The arguments presented above for inkjets in section 4.3 are equally valid for this design – the device would be limited by its blocking pressure hence cannot be used as a self-aspirating pump.

(b) As an atomizer

In this mode fuel is forced through a nozzle (a slot nozzle in this case) by the pressure of the fuel itself. The electrostatically actuated membrane is used to excite a high frequency

disturbance of the jet / sheet as it leaves the device, which promotes a more rapid atomisation and smaller droplets. The paper [18] does not report at what frequency the membrane was actuated. The devices also made use of a transverse air jet across the nozzle to promote atomization – it is not clear how well they would perform without this air. This seems a promising way of producing small droplets, but if used to inject into a rocket engine, there would be no means of modulation the flow rate. An additional concern is that a voltage of 1000V is required across the electrodes to actuate the membrane, which may exceed the dielectric breakdown threshold of some fuels.

To avoid the possibility of a dielectric breakdown a piezo – actuated membrane can be used.

5.2 Assessing excitation for enhanced atomisation

A piezo-actuated MEMS atomizer has been modelled to study the influence of the membrane movement on the flow characteristics.

The MEMS atomizer schematic is reported below

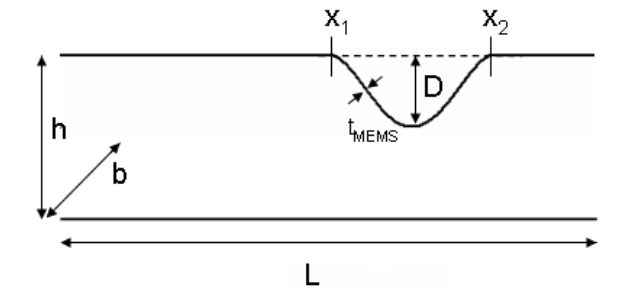

Figure 15 – MEMS atomizer schematic

The governing equations are the ones for a quasi-monodimensional non viscid flow with cross section area that varies with time and space

$$\begin{aligned} &\rho\frac{\partial A}{\partial t}+\rho v\frac{\partial A}{\partial t}+\rho A\frac{\partial v}{\partial x}=0 \\ &\rho A\frac{\partial v}{\partial t}+\rho A v\frac{\partial v}{\partial x}+t_{MEMS}\rho_{MEMS}\frac{1}{b}\frac{\partial^2 A}{\partial t^2}=-\frac{\partial pA}{\partial x} \end{aligned} \tag{9}$$

where A is the cross section area, ρ and v the density and velocity of the fluid, t_{MEMS} and ρ_{MEMS} the thickness and density of the actuated membrane and D its maximum displacement.

The membrane motion has been represented like a 4-th order polynomial (so that in x_1 and x_2 the first derivative of A with respect to x is always continuous) sinusoidally varying in time

$$A(x,t)=\begin{cases} bh & x<x_1 \\ bh-\dfrac{16Db}{(x_1-x_2)^4}(x-x_1)^2(x-x_2)^2\sin(\omega t) & x_1\le x\le x_2 \\ bh & x>x_2 \end{cases} \tag{10}$$

The solution for the velocity has been calculated analytically

$$v(x,t)=\begin{cases} v_i & x<x_1 \\ \dfrac{bh}{A(x,t)}\left[\dfrac{16D}{bh(x_1-x_2)^4}g(x)\cos(\omega t)\omega+v_i\right] & x_1\le x\le x_2 \\ \dfrac{bh}{A(x,t)}\left[\dfrac{16D}{bh(x_1-x_2)^4}g(x_2)\cos(\omega t)\omega+v_i\right] & x>x_2 \end{cases} \tag{11}$$

where v_i is the initial velocity due to the pressure difference along the injector and g(x) is a function defined like

$$\begin{aligned} v_i &= \sqrt{\frac{2\Delta p}{\rho}} \\ g(x) &= \int_{x_1}^{x_2}(x-x_1)^2(x-x_2)^2\,dx \end{aligned} \tag{12}$$

while the pressure has been calculated numerically integrating the second of (9)

$$p(x,t)=\frac{1}{A}\left[p_i bh-\int_0^x \rho A\frac{\partial v}{\partial t}dx-\int_0^x \rho Av\frac{\partial v}{\partial x}dx-\int_0^x t_{MEMS}\rho_{MEMS}\frac{\partial^2 A}{\partial t^2}dx\right] \tag{13}$$

As can be seen from (12) and (13) both the velocity and the pressure at the exit of the injector depend directly on the excitation frequency ω and on the maximum displacement of the membrane D. Hence during the membrane design phase the choice of these two parameters must be done carefully to avoid big velocity and pressure oscillations that can excite combustion instabilities inside the combustion chamber.

As will be explained in §7.2 the droplet size is mainly dependent on the jet velocity and on the injector diameter. In a MEMS atomizer like the one described above the diameter and velocity are of the same order of magnitude than a conventional injector hence there should not be any improvement in the droplet size.

What a MEMS atomizer can do is to accelerated the breakdown process being able to produce droplets in a shorter time (hence in a shorter space) compared to a conventional injector giving the possibility of reducing the chamber length saving mass or, keeping the same chamber dimensions, having a more complete and efficient combustion.

The time required for the breakdown can be expressed as [25]

$$t = \frac{1}{\beta}\ln\left(\frac{h}{2\delta}\right) \qquad \beta = \sqrt{\frac{\omega^2 \frac{\rho_A}{\rho_L} - \frac{\omega^3}{\bar{v}^3}\frac{\sigma}{\rho_L}}{\tanh\left(\frac{\omega}{\bar{v}}\frac{h}{2}\right)}} \tag{14}$$

where β is the grow factor, ρ_A and ρ_L the density of the liquid and of the surrounding gaseous medium, σ the liquid surface tension, h the initial thickness of the jet, $\bar{v}$ the average liquid velocity and δ the initial disturbance in the jet thickness.

In a conventional injector the term $\ln\left(\frac{h}{2\delta}\right)$ has a value close to 12 [36] while for a MEMS injector it can be expressed as

$$\delta = \frac{h}{2}\left(1 - \sqrt{\frac{\bar{v}}{v_{max}}}\right) \qquad \ln\left(\frac{h}{2\delta}\right) = \ln\left(\frac{\sqrt{v_{max}}}{\sqrt{v_{max}} - \sqrt{\bar{v}}}\right) \tag{15}$$

In a conventional injector the jet vibration frequency is

$$f_1 = \frac{\rho_A \bar{v}^3}{2\pi\sigma} \tag{16}$$

while in a MEMS it can be changed to minimize the breakdown time. This optimization process has been performed assuming to have a MMH/NTO 40N thruster with a chamber pressure of 7 Bar with a 2 Bar pressure drop along the injector plate. The result are shown below in Table 2

Thrust	40 N	I_{SP}	300 s
mixture ratio O/F	1.6	velocity at the injector exit	MMH 21.44 m/s NTO 16.6 m/s
Required $\dot{m}_{MMH}$	0.005 Kg/s	Required $\dot{m}_{NTO}$	0.008 Kg/s
ρ_{MMH}	870 Kg/m^3	ρ_{NTO}	1450 Kg/m^3
injector height h	45 μm	membrane thickness t_{MEMS}	37 μm
injector base b	45 μm	membrane length x_1-x_2	1.5 mm

Voltage applied to each membrane ΔV	11.1 V	mass flow rate of a single NTO injector	$4.89 \cdot 10^{-5}$ Kg/s	
mass flow rate of a single MMH injector	$3.78 \cdot 10^{-5}$ Kg/s	number of NTO injector	164	
number of MMH injector	132	blocking pressure	10 Bar	
injector plate diameter	4.1 mm	optimal exciting frequency	MMH	16500 Hz
			NTO	9700 Hz
Expected droplet size		50 – 100 μm		

Table 2 MEMS injector design for a 40 N thruster

The grow factor for MMH and NTO is showed for both this injector and a conventional one

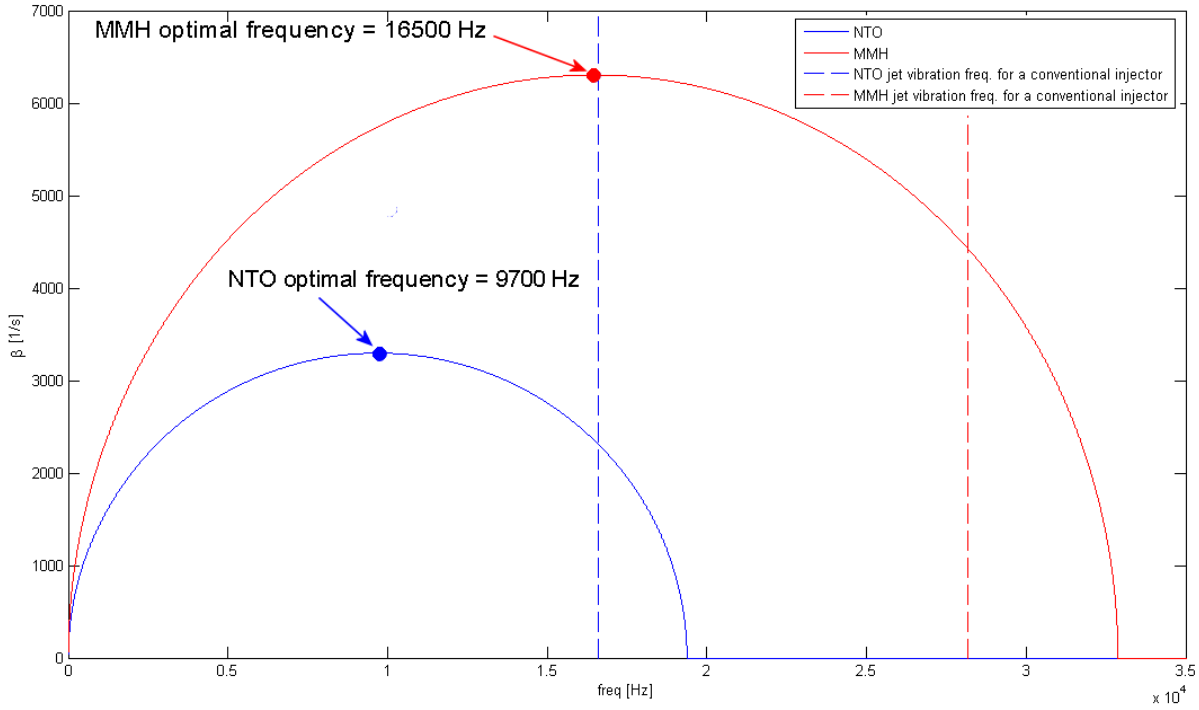

Figure 16 – Grow factor for a MMH and NTO

Hence the optimal excitation frequency is 16.5 KHz for MMH and 9700 Hz for NTO. The choice of D and of the membrane length and thickness has been made to obtain a blocking pressure of 10 Bars (Eq (6),(7))and to reduce the pressure and velocity oscillation at the exit of the injector.

The velocity and pressure variation with time and frequency at the exit of the injector are show in Figure 17Figure 19

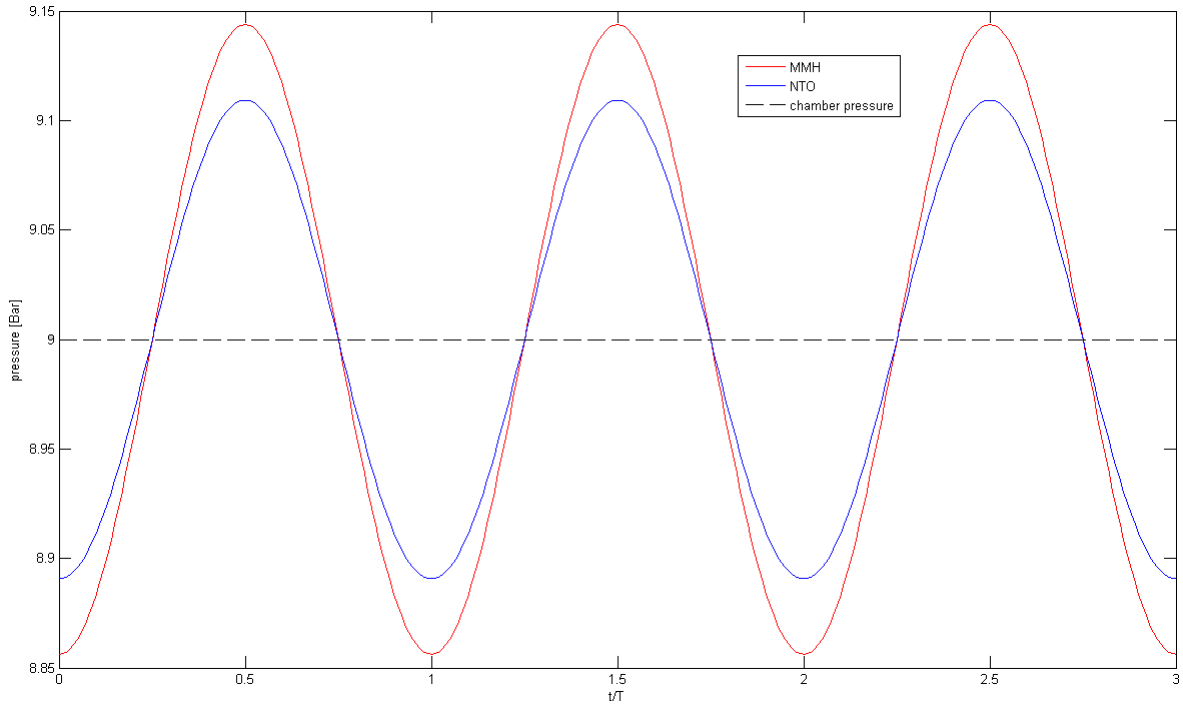

Figure 17 pressure trend with time at the exit of the injector, f_{MMH} = 16500 Hz f_{NTO} 9700 Hz

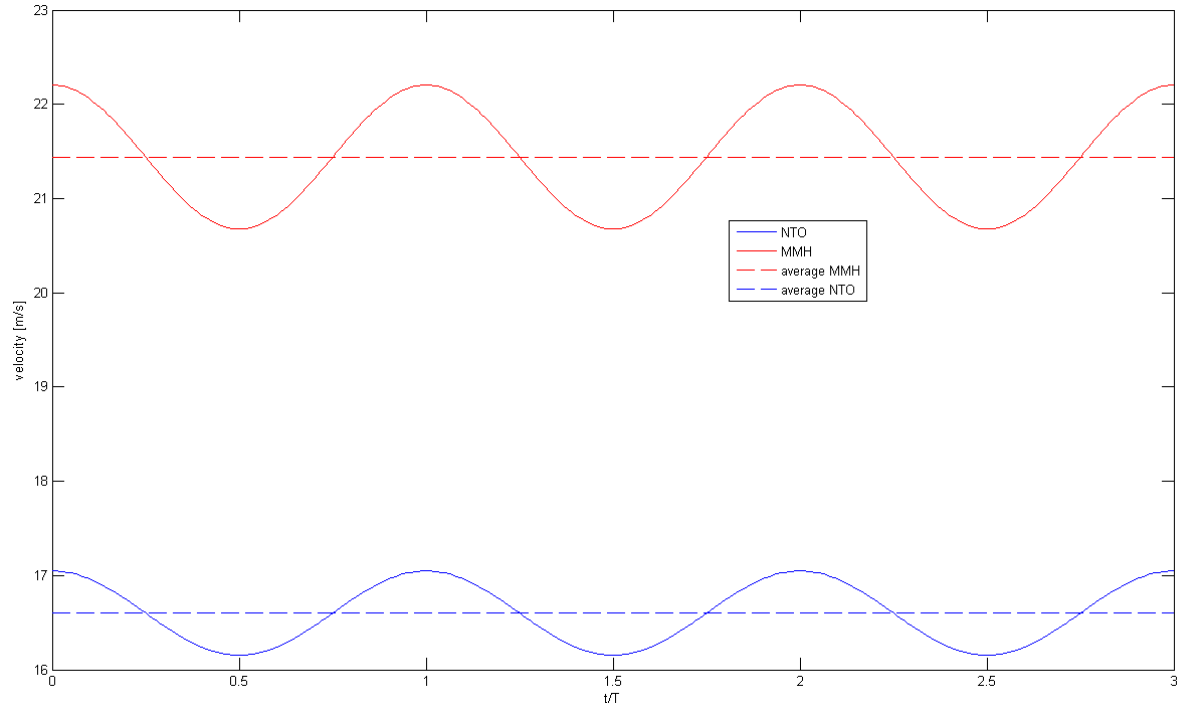

Figure 18 velocity trend with time at the exit of the injector, f_{MMH} = 16500 Hz f_{NTO} 9700 Hz

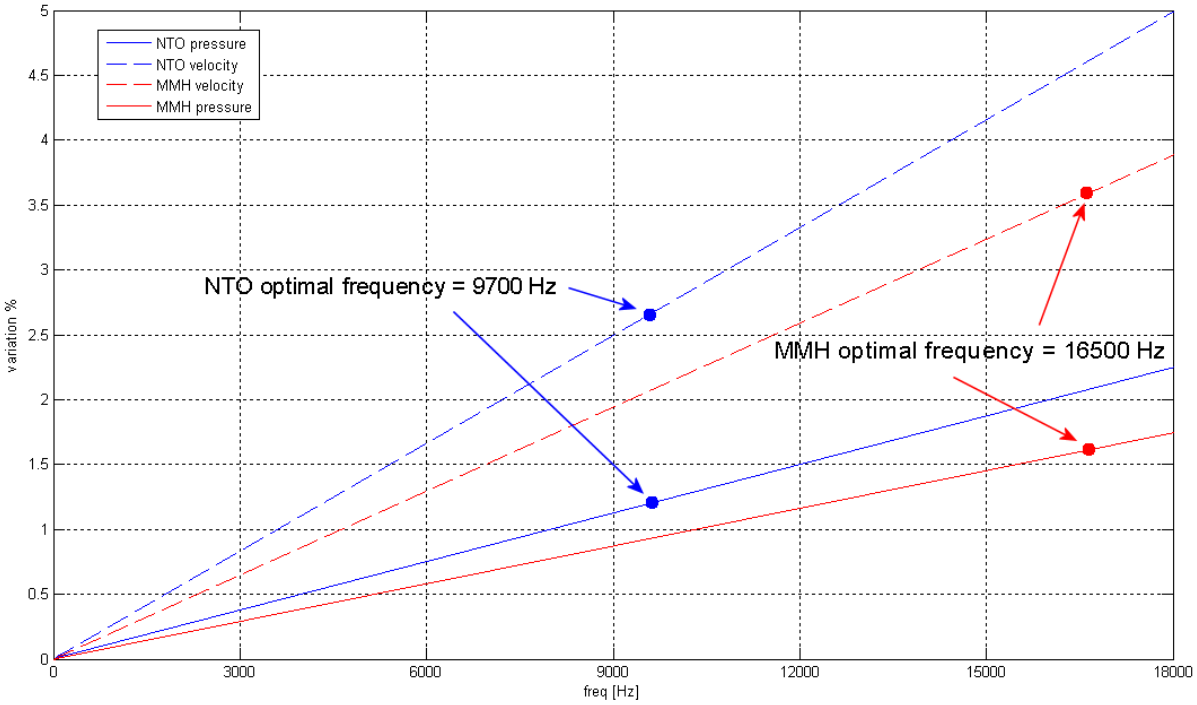

Figure 19 velocity and pressure trend with frequency at the exit of the injector

Using the optimal frequency the ratios between the break-up lengths with a conventional injector and with a MEMS atomizer are respectively 4.23 for MMH and 3.94 for NTO.

In conclusion the MEMS atomizer shows the possibility of sensibly reducing the break-up length (four times shorter) allowing a combustion chamber length reduction or a combustion efficiency increase although the droplet size should not be sensible of any increase.

Experimental tests are needed to confirm the theoretical prediction and to verify the actual droplet size.

5.3 Other methods of enhancing atomisation

Pulse Detonation Engines (PDEs) require very fine sprays of droplets to produce a mixture that can successfully be detonated. We investigated PDE literature to see if any techniques were employed that could be adapted for a rocket injector. The review by Roy [19] is particularly informative. Several main schemes are used: (a) Using gaseous fuels; (b) Using air-blast atomisers (a high velocity air stream breaks apart a sheet of fuel); (c) prior to injection the fuel was heated and pressurized so that evaporation was very rapid; (d) fuels were combined, and allowed to flow down a tube to permit evaporation and mixing before

reaching the combustion chamber; (e) High pressure fuel was injected using diesel engine type fuel injectors. Option (e) will be investigated chapter §7.

Roy notes,

> "To our belief, the problem of detonation initiation in close-to-practical PDEs with homogeneously mixed [fuel air mixtures] approaches its successful solution. In view of it, the problems of organizing efficient filling of the combustor and nearly-perfect mixing become crucial. Unfortunately, these issues are not properly tackled so far."

And also,

> "Nowadays, it is absolutely clear that there is no fundamental constraints in applying repeatedly propagating confined detonations for producing thrust. Thermodynamic efficiency of pulse detonation thrusters is considerably higher than that of other conventional thrusters based on combustion, particularly at subsonic flight at relatively low altitudes. In view of it, both air-breathing and rocket propulsion seem to receive a chance of getting a long-expected breakthrough in efficiency, and, as a consequence, in increased range, payloads, etc. The additional benefits of an ideal PDE are: simplicity of design and low weight."

US patent 5,873,240 for a "Pulsed Detonation Rocket Engine" seems to employ a coaxial or air-blast atomiser (its not clear), as shown in Figure 20.

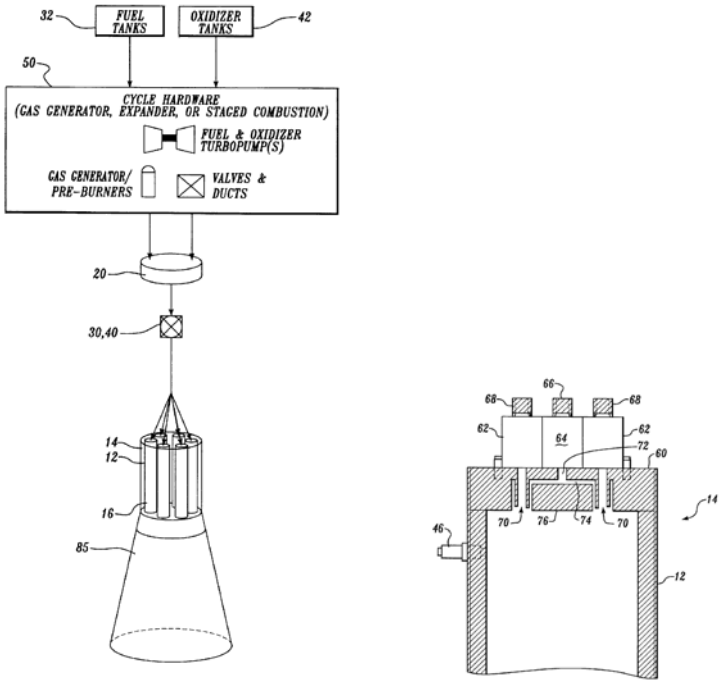

(a) overall system (b) Injector - with oxidiser and fuel channels, 70, 72

Figure 20 Diagrams from US Patent 5,873,240: Pulsed Detonation Rocket Engine.

6 Electrospray injectors [37,38]

A way of obtaining a very small droplet size is to use the electrospray phenomenon. This phenomenon has been discovered in 1914 and consists in the broke up into fine droplets of a liquid at the end of a capillary thanks to the application of an electric field. In this kind of device the droplet size is related to mass flow rate by a power law hence to obtain a small droplet size and achieve the required mass flow rate a MEMS fabricated array of nozzles (multiplexed electrospray) can be used.

This configuration is represented in Figure 21

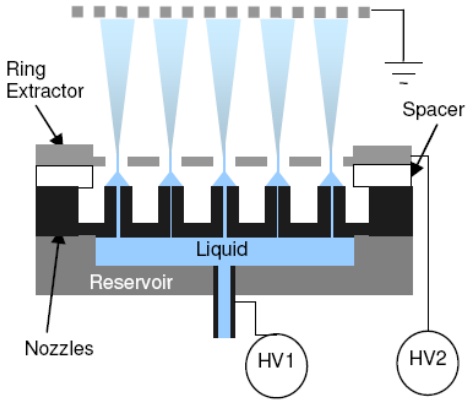

Figure 21 – MEMS array of elecrospray nozzles [37]

The nozzle array and the electrode are connected to a voltage source to create a strong electrical potential difference between the two. Due to electro-hydrodynamic and capillary forces a Taylor-cone forms at the tip of each nozzle. If the applied electric field exceeds a threshold value small charged droplets will be ejected. Then the droplet repelling each other because of their charge form a monodispersed spray.

The performances of this kind of injector published in [37] are extremely interesting. Using a 91 nozzle array whose configuration is shown in Figure 22

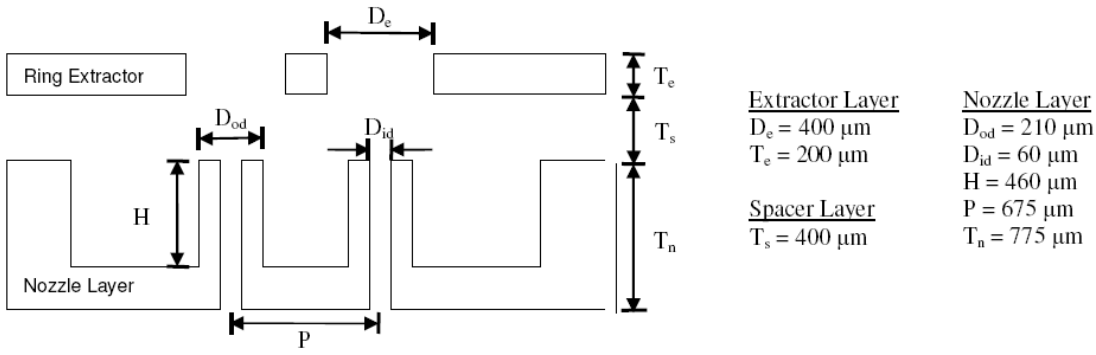

Figure 22 multiplexed electrospray configuration used by Deng et al. [37,39,40]

they have achieved droplet size of ~ 11μm without any sensible pressure drop along the nozzles (~ 2 kPa) with sub-mW power levels and obtaining a volumetric flow rate of 5.55 mm^3/s .

This configuration has been applied to design the injector plate of a 4N and of 40N thruster. The results are reported in Table 3

	Waits and Jankowsky multiplexed electrospray array[37]	4 N thruster	40 N thruster
Specific impulse	-	300 s	300 s
volumetric flow rate	5.55 mm^3/s	1.12 cm^3/s	11.2 cm^3/s
number of nozzles	91	18345	183450
power required	< 1 mW	< 2W	< 20W
mean droplet diameter	11 μm	11 μm	11 μm
injector plate radius	-	~ 5 cm	~ 16 cm

Table 3 Multiplexed electrospray application to a 4N and 40N thruster

As can be seen the power consumption is affordable both for a 4N and a 40N thruster, the droplet size is extremely small the only problem is the high number of nozzle and the relatively high injector plate radius. To reduce this the mass flow rate of each injector can be increased hence reducing the total number of nozzle but at the same time increasing the droplet diameter. For example in JP8 fuel the relation between mass flow rate and droplet size is[37]

$$D = \dot{Q}^{0.5} \tag{17}$$

hence if the mass flow rate for a single nozzle is multiplied by four, accordingly reducing the number of injector, the droplet size will be only doubled increasing from 11 to 22 μm and still being very attractive.

A big advantage of this kind of injectors is that such small droplet particle has been proved to produce a cleaner combustion [38] and that the flow rate is proportional to the applied voltage hence varying this voltage the mass flow rate can be changed easily throttling the thruster. The level of throttling that can be achieved has to be verified by further analysis. The controllability of the mass flow rate via the applied voltage gives also the possibility of performing real time combustion instability control.

The problem related with the use of an electrospray injector is the unknown effect that this kind of injection will have on the combustion instabilities and whether or not the usual pressure drop across the injection plate will be needed. Another question mark is the effect of charged particle in the combustion processes.

7 Diesel injectors

7.1 Introduction

In this section we consider whether the injectors found in diesel engines could be useful as bipropellant rocket injectors. The basic principle of these systems is that a carefully metered quantity of fuel is injected in a short time; the nozzle size and pressure are such that a high degree of atomisation is attained.

Diesel injectors were first produced in the 1920's and have evolved considerably since then. Figure 23 shows a typical configuration with an in-line injection fuel pump. This design uses an impulse from a camshaft to create a high-pressure pulse of fuel. This pressure is sufficient to push open the spring loaded valve at the tip of the spray nozzle.

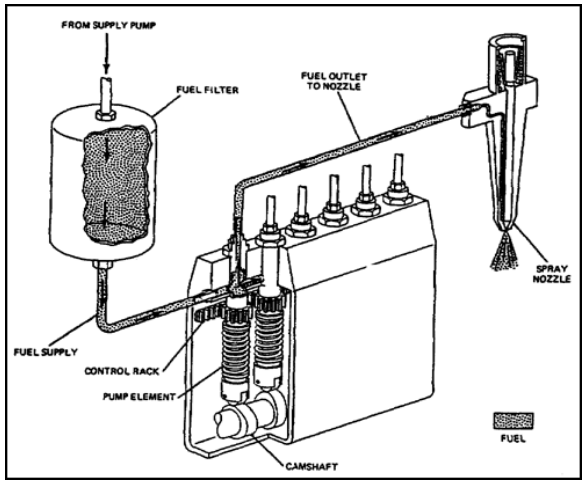

Figure 23 In-line diesel injection (from [20])

The first common rail injection system was produced in 1997 [21]. This configuration permits full electronic control of the injection event. A fuel pump operates continuously, pressurising fuel to typically 1000 bar (recent designs operate at even higher pressures) and feeds it into the common rail where it is held ready for injection. Individual injectors feed fuel directly into the engine's combustion chambers. The injectors are controlled electronically, so the quantity of fuel injected is independent of engine or pump speed, and can be fired at any point in the cycle.

Figure 24 shows a typical fuel injector, actuated by a solenoid. It is important to note that the action of the solenoid does not directly open the nozzle. (a) When the nozzle jets are closed, the pressure of the fuel acting on the nozzle needle (11) in the valve-control chamber (8) is greater than that acting on the shoulder of the nozzle needle. This presses the needle against its seat and no fuel flows through the nozzle. (b) To open the needle valve, the solenoid is actuated, lifting the valve-ball (5). Fuel flows out of the control chamber (8), and the reduced pressure there allows the needle to lift.

This indirect method of opening the needle valve reduces the amount of force and displacement that needs to be supplied by the actuator. The extra fuel, passing through the fuel-return outlet (1) is collected for re-use. The injectors are machined to a very high standard, with clearances of as little as 2μm round the injector needle. On a typical car engine the injection quantity can be controlled over the range $1mm^3$ (for a pre-injection) to $50mm^3$ (full load delivery), with fuel velocities of 60m/s and injection times of 1ms or less possible [21].

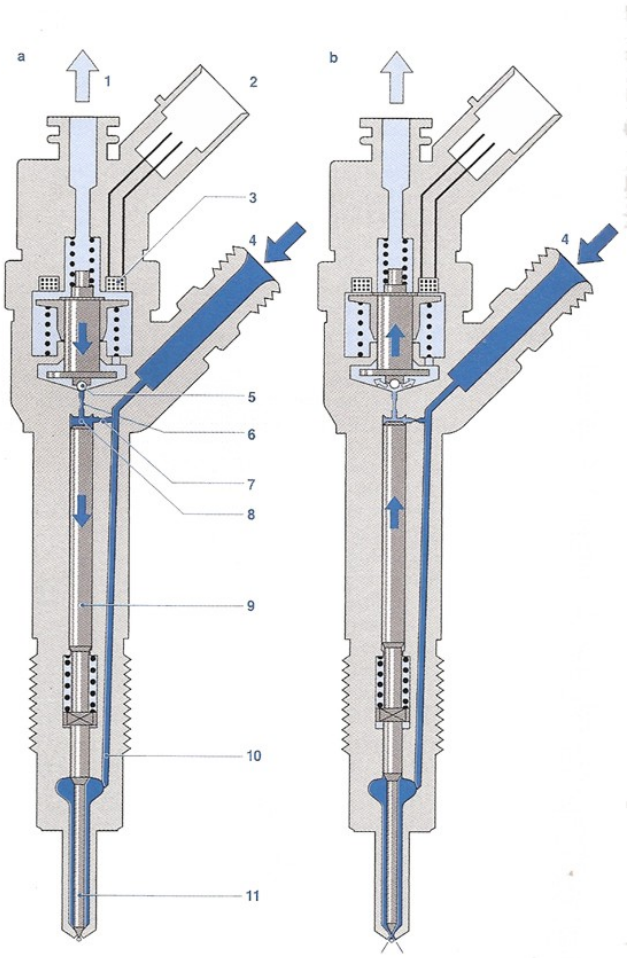

Figure 24 Common Rail Fuel injector (from Bosch [21], pp. 310)

Piezoelectric transducers have replaced the electromagnetic actuator on some more recent designs. The higher force, and quicker response time of a piezoelectric transducer means that the valve can be opened and shut more quickly. This results in a higher average velocity and hence smaller droplet sizes [22], and also permits more precisely metered quantities of fuel. Thus piezoelectric injectors can produce cleaner, more efficient engines.

Figure 25 shows two nozzle designs. The sac nozzle is widely used and produces a more uniform flow across the holes, but after injection has finished the remaining fuel in the sac volume drips out and contributes to sooty emissions [23].

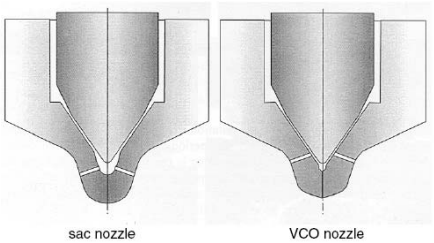

Figure 25 Injector nozzles (from Bae [23])

Figure 26 shows some typical spray data, and also illustrates how the droplet size decreases if the fuel pressure is reduced (Y and R are the axial and radial distances from the injector axis respectively). Note how much smaller the final droplets are than the initial size of the nozzle hole, due to the high velocity atomisation.

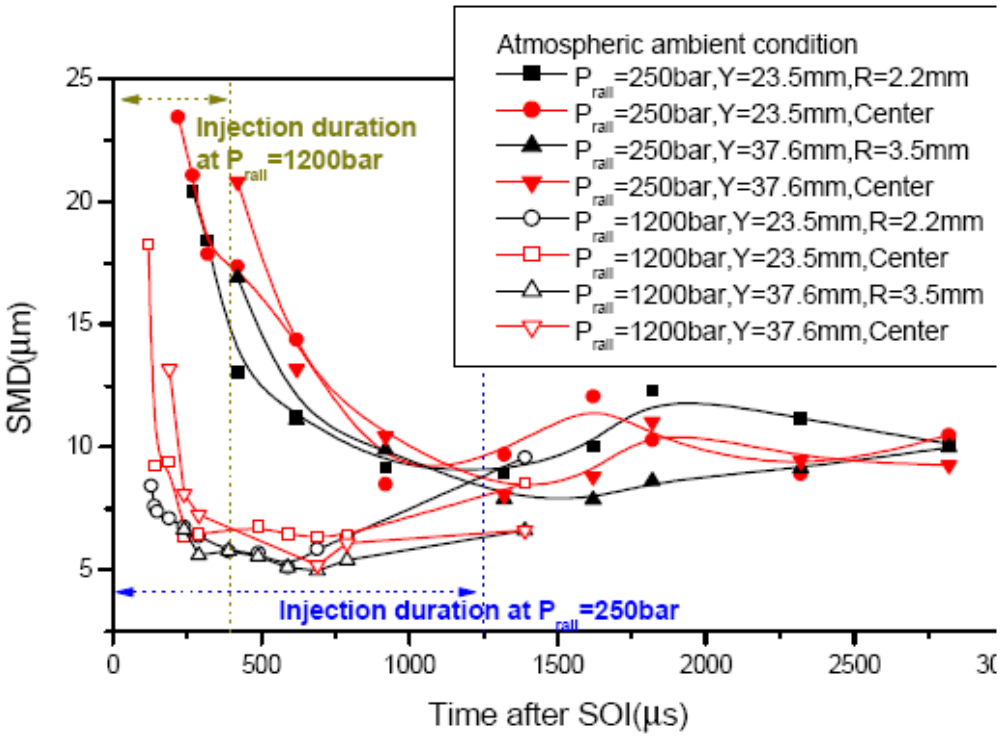

Figure 26 Effects of injection pressure and time on SMD of the spray from VCO nozzle (0.144mm x 5hole) (from Bae [23])

7.2 Droplet size

Although some simple empirical relations exist for predicting the type of spray produced by atomiser designs, to obtain predictions accurate enough to predict how the combustion will progress will generally require either computational fluid dynamics or experiment – or both.

Changing the size and distribution of droplets will have significant effects on the combustion in the chamber. In a plain orifice injector under high pressure the droplets can be very much smaller than the injector nozzle diameter – e.g. in Figure 26 above, droplet sizes can be less than 0.1 of the nozzle diameter. Compare this to typical ratios of 0.2 to 0.4 for impinging injectors in a rocket engine [24]. Santoro [24] comments on several factors effecting stability in impinging injectors, noting: (a) that reducing droplet size will bring combustion closer to the injector face and hence reduce stability by coupling the combustion

more closely to the injector dynamics; (b) that "it is reasonable to expect that stability will be enhanced if there is a wide distribution of drop sizes because any present effects of resonant burning can be essentially neutralized by different-sized drops that release most of their chemical energy out of phase with the drops that are burning in resonance with pressure oscillations."; and (c) that "The frequency with which periodic surface waves and ligament structures are formed have a marked similarity to the highest possible combustion instability frequency as predicted by the [Hewwitt] stability correlation.". By shifting to using active injection points (a) and (b) suggest that we risk increased combustion instability, but (c) suggests that by working in the atomization break-up mode (see Figure 27, below) there may be less excitation of instability modes (though care must be taken not to actuate injectors at frequencies that would excite instability modes).

Another consequence of reducing droplet sizes would be that as the combustion area moved closer to the injector face, the temperature stresses on the injectors would be increased.

US patent 6,102,299, a "Fuel injector with impinging jet atomizer" combines fuel injection with jet impingement. Such a scheme may well be necessary to achieve sufficiently small droplets at the pressures considered in the following section, and also to promote good mixing of the fuel and oxidiser.

7.3 Applicability to rockets

The fine atomisation, and degree of control afforded by diesel injectors make them attractive for producing rocket motors that are more efficient, cleaner, with the possibility of controlling in real time combustion instabilities and throttle control. The main problem is whether fuel pressure can be reduced to a value that can be produced in a rocket while maintaining sufficient flow and atomisation, and also whether existing technology could be made use of to implement such a system.

If fuel of density ρ_L, is forced through a nozzle by a pressure differential ΔP, the velocity of the resulting jet can be approximated as [25],

$$v = C_D \sqrt{\frac{2\Delta P}{\rho_L}} \tag{18}$$

where C_D is the discharge coefficient (see Lefebre [25] for the effect of Reynolds number and orifice geometry on C_D)

The break-up of a jet issuing from a plain orifice can take one of several modes depending (ignoring the effect of nozzle geometries and upstream flow characteristics) on the velocity of the jet and the properties of the fuel and ambient atmosphere; this is illustrated in Figure 27. At low velocities the Rayleigh mode, caused by the growth of unstable perturbations of the jet, produces drops approximately 1.9 times the size of the orifice. As the velocity is increased interactions with the surrounding gas produce the first, and second wind-induced modes and finally the atomization mode is reached which is also much influenced by cavitation and turbulence in the initial jet. In the first wind-induced mode the droplet size is of the same order as the orifice, while in the subsequent modes the droplet sizes are very much smaller (as seen above in Figure 26). If such an orifice were to be used in a rocket injector, we would want to be in the second-wind induced or atomization modes.

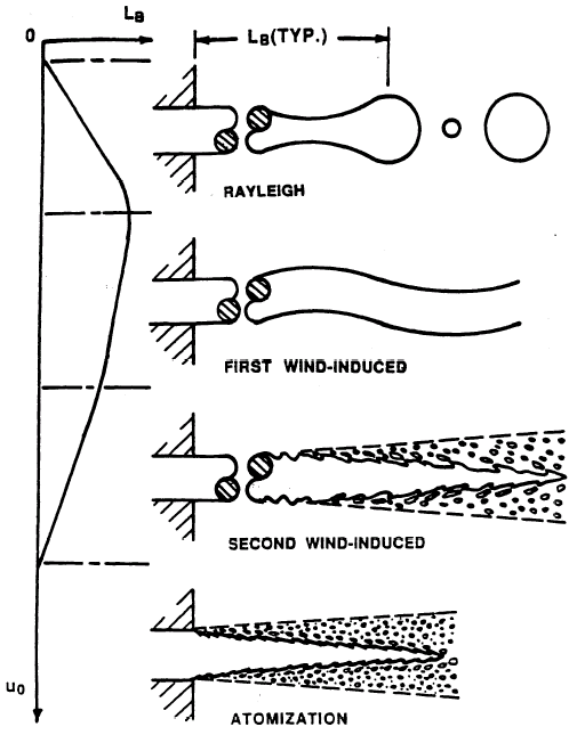

Figure 27 Mechanical jet break-up regimes (from Faeth [26])

Lin and Reitz [27] have suggested a scheme for determining which break-up mode is likely for a given system:

Break-up mode 1 The Rayleigh break-up region: $We_L<8$ and $We_G>0.4$ or $1.2+3.41\ Z^{0.9}$

Break-up mode 2 The first wind-induced region:

$1.2+ 3.41\ Z^{0.9} < We_G < 13$

Break-up mode 3 The second wind-induced region:

$13 < We_G < 40.3$

Break-up mode 4 Atomization region:

$We_G > 40.3$

Where the Weber number (gas) is given by

$$We_G = \frac{\rho_G v^2 D}{\sigma} \tag{19}$$

where D is the diameter of the nozzle, σ is the surface tension and ρ_G the density o the ambient gas. The Weber number (liquid) is given by:

$$We_L = \frac{\rho_L v^2 D}{\sigma} \tag{20}$$

And the Ohnesgorge number,

$$Z = \frac{\mu}{\sqrt{\rho_L \sigma D}} \tag{21}$$

Using these we can explore various combinations of fuel pressure and nozzle diameter and see what degree of atomization can be produced.

The combustion chamber gas density was calculated using the ideal gas law, and Table 4 lists the other material properties used in the calculations. The discharge coefficient, C_D, was approximated from a graph given in Lefebvre [25] which relates it to Reynolds number and nozzle geometry (a nozzle width to length ratio of 0.25 was used).

Fuel	Dynamic viscosity (kg/(ms))	Density (kg/m^3)	Surface Tension (kg/s^2)
MMH	7.71E-04	8.78E+02	3.43E-02
NTO	4.10E-04	1.44E+03	2.63E-02
LOX	2.2E-04	1.15E+03	2E-02
H2	1E-05	71	0.2E-02
RP1	2.4E-03	8.3E+02	2.8E-02

Table 4 Fuel properties

Figure 28-30 show the results for a range pressures and orifice diameters. The vertical axis indicates the relative pressure drop along the injectors while the horizontal indicates the

chamber pressure in Bars. The solid lines mark the transition between break–up modes 2 and 3 while the dashed one between modes 3 and 4.

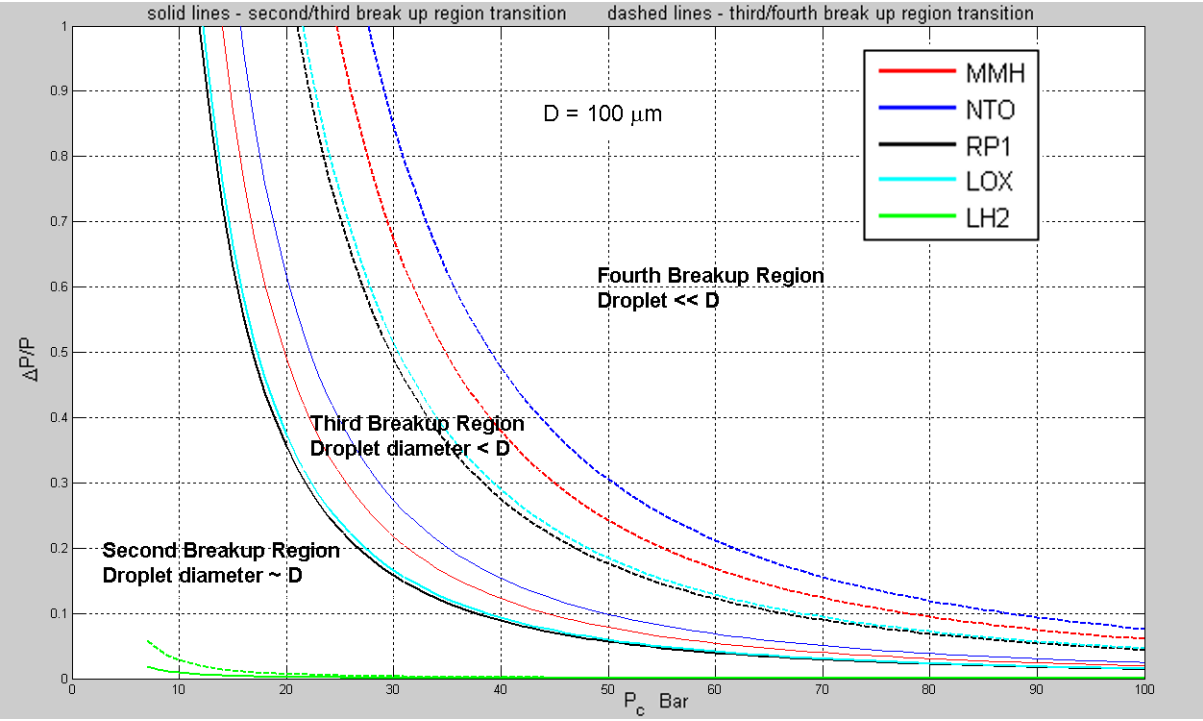

Figure 28 – Break-up modes for different pressures and pressures drops D=100μm

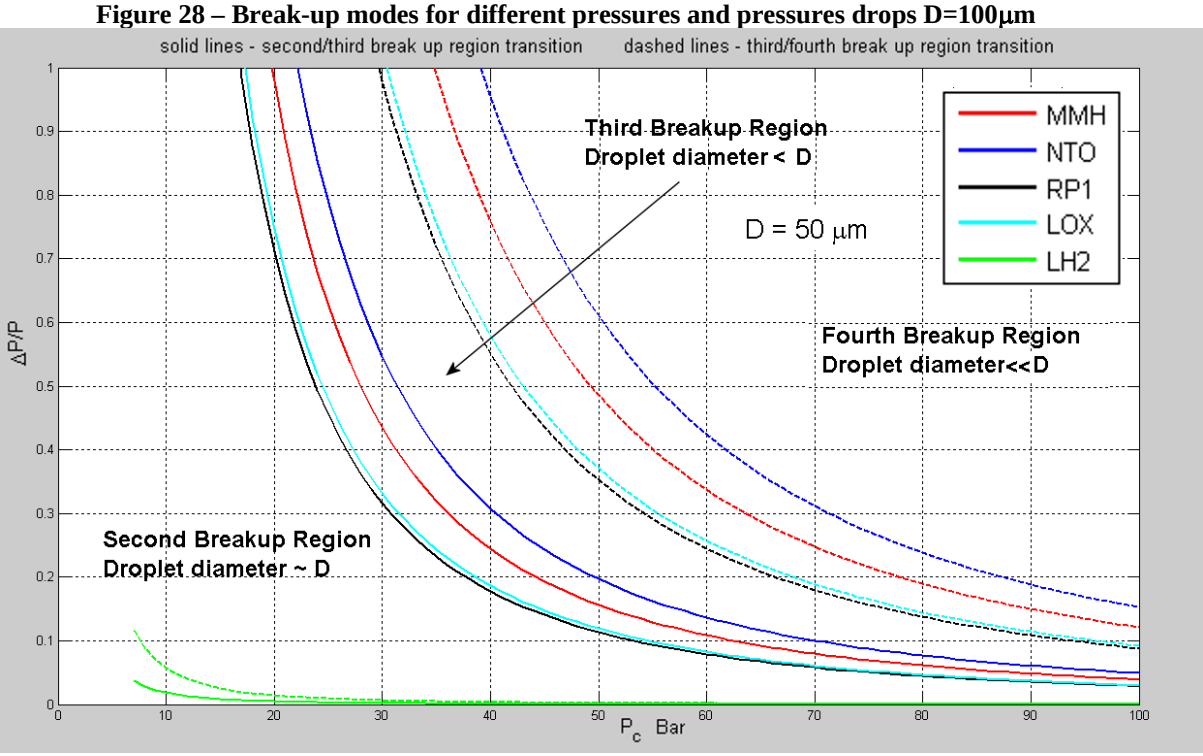

Figure 29 - Break-up modes for different pressures and pressures drops D=50μm

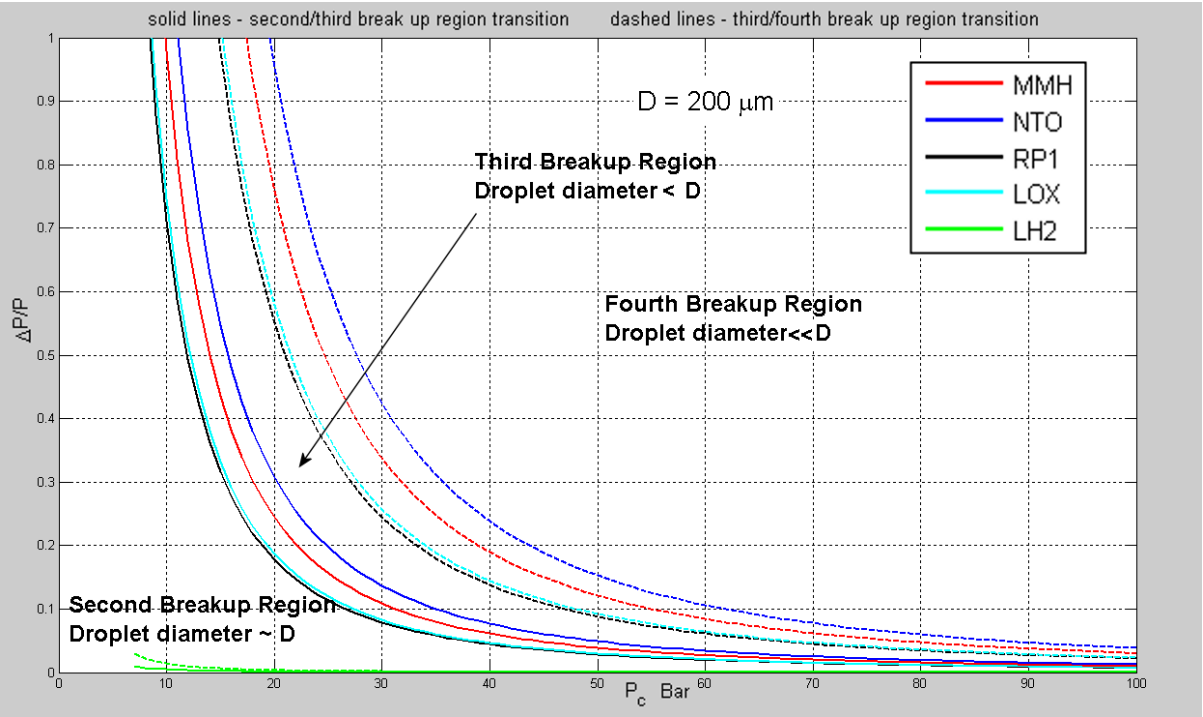

Figure 30 - Break-up modes for different pressures and pressures drops D=200μm

As can be seen because of the high pressure drop required these kind of injectors are practically usable only on big thrusters with a high chamber pressure. Assuming to be interested in break up mode 4 (the one providing the smallest droplet size) depending on the propellant selection and on the injector diameter size we need chamber pressures between 45 and 90 Bars if the pressure jump in the injectors is 20% of the chamber pressure.

The choice of the injector diameter must hence be done taking into account the droplet size needed but also the pressure drop available for the injectors and the maximum number of injector that can be reasonably allocated in the injector plate.

A way to reduce the number of injector is to increase the numbers of nozzles that each diesel injector has. Commonly each injector has 5 nozzles but this number could be raised reducing the number of injector without affecting the performance of the injector.

7.4 Fuel Injector Conclusions

It would seem that fuel injectors could feasibly be incorporated into a rocket engine. If this injectors are piezoelectrically actuated, since energy is only consumed when switching between on and off states it is likely that they would offer a very low power consumption.

Piezoelectric actuators have a very fast response time, and this opens up the possibility of using active control to reduce combustion instabilities in the combustion chamber.

Further study based on computational fluid dynamics or experiment would be required to form an accurate prediction of the distribution of droplet sizes

The mode of operation of such a rocket engine would be quite different to an internal combustion engine, where the high pressure is used to inject all the required fuel in only a short interval. In a rocket with actuated injectors we envisage most of the injectors firing most of the time – active control could then be used to monitor and control any combustion instabilities, and to avoid any hot-spots on the chamber walls.

We must question whether incorporating injectors would increase the performance of a rocket sufficiently to justify the additional complexity and weight. The main advantages would be very good throttling control (varying the mass flow rate and hence the trust from zero flow up to the maximum level), through adjusting the duty cycle, and the possibility of active instability control. Increased efficiency is also likely due to smaller droplets.

7.5 Active injection – a design concept

This section presents a proposed design that demonstrates a possible configuration for an active injection system for the 50 KN RS72 thruster. Only basic calculations have been performed to assess its performance – the in depth analysis and refinement of this design is proposed as future work.

The design is shown in Figure 31, and key properties of the design are listed in Table 5. It comprises a number of piezoelectrically actuated injectors, each injector having a number of nozzles. The overall diameter of the system and of each injector as marked on the figure is only an estimate of what might be feasible. Since the pressures involved are much lower than those found in a diesel engine, the piezoelectric actuators act directly on the nozzle needle. Using a similar, but longer, stacked piezoelectric actuator to the one described by Yang [30], a stroke distance on 50 μm will occur at an actuation voltage of 60V for an actuator length of 50mm. Further work is required to determine if this is sufficient to maintain the predicted flow rates, and also to ensure that the actuator supplies sufficient seating force to prevent leakage (see Yang for discussion of this). See Figure 25 for a nozzle design.

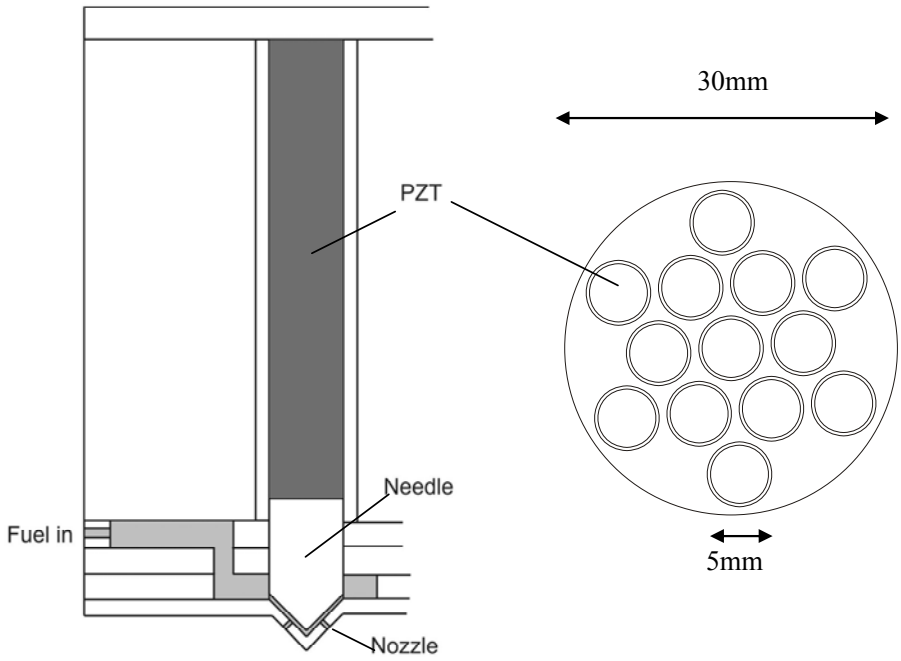

Figure 31 Proposed Active Injector system (not to scale)

An alternative configuration would be to use an injector design similar to those used in diesel engines, where the actuator moves a valve that enables the fuel pressure to move the nozzle needle (see section 7.1). This is more complex, but would require less electrical power and a lower voltage.

An advantage of this configuration is that the nozzle and nozzle needle are both robust, and can safely be exposed to the atmosphere of the combustion chamber. If a membrane type valve design (e.g. Yang [31]) were used the membrane would be at risk.

304 or 307 Stainless steel is proposed as the material for the injectors as it is compatible with both MMH and NTO [32]. To prevent chemical interaction of the fuels with the PZT actuators, we suggest that a PTFE coating completely surround the actuator. Further study is required to see if this would be sufficient to protect the PZT. Also thermal considerations may require a different material for the nozzles.

The method of manufacture is not considered here, but a combination of milling, and EDM for several bonded layers would produce a suitable result.

The number of fuel and oxidiser nozzles has been tailored to provide close to the optimum oxidiser to fuel mass ratio of 1.6 at full thrust. Since this scheme provides the possibility of active control, the total number of nozzles supplied in the design exceeds the

minimum number required so that even at maximum thrust there is the possibility of tailoring the spatial distribution of the oxidiser/fuel ratio.

The optimum spatial arrangement of injectors has not been considered – further work is required to determine a useful arrangement that would enable liquid cooling of the walls, and suitable spatial distributions of oxidiser/fuel ratios over a wide range of output thrusts.

	MMH	**NTO**
Total thrust	50 KN	
Chamber Pressure	60 bar	
Pressure drop	12 bar (20% of chamber pressure)	
Nozzle diameter	100μm	
Fuel velocity (m/s)	42	33
Number of nozzles	10000	5000
Nozzles per injector	10	10
Number of injectors	1000	500
Maximum mass flow rate (Kg/s)	11.6	7.5
Break-up mode (see above)	Second-wind induced / atomization	
Droplet diameters, SMD	Further study required: 30μm?	
Injector plate diameter	~ 0.5 m	

Table 5 Active Injector Design parameters

The power consumption can be estimated using data presented by Yang. To hold open all 1500 injectors would consume about 45W (this is dissipated through leakage currents in the actuators). Additional power is consumed to change the state of the actuators. It is envisaged that in most modes of operation, most injectors would be held in a steady state most of the time (nozzles can be held half open at no extra power cost), with some small adjustments for control purposes.

To summarise, the following main areas would need investigation to further this design:

(a) Model flow through the entire design, checking whether this design provides sufficient opening distance, and sufficient seating force for leak free operation.

(b) Experiments and further design to ensure reliable injector operation, in particular: chemical isolation of PZT from fuels, possible lubrication additive to fuel, and investigation of clogging and filtration.

(c) Use experiments or modelling to determine the distribution of droplet sizes and droplet penetration the injectors would produce.

(d) Use experiments or modelling to assess the effects of droplet size changes and other parameters on dwell times of unburnt fuel, mixing, combustion stability, etc.

(e) Thermal modelling to ensure materials are not over stressed.

(f) Overall system modelling to determine appropriate layout of injectors to provide required functionality over a range of output thrusts, and effective active control.

8 Pump and Nozzle Materials and manufacture

Micromachining and MEMS (Micro Electro-Mechanical Systems) have traditionally been heavily focussed on silicon as a substrate. However, a range of other materials can be engineered at a small scale, and can be found in many micro-pump and micro-valve designs. For instance, micro-pumps have been reported with brass, glass, silicone, steel, silicon and polyimide membranes.

The boiling points of MMH and NTO fuels are 87 and 21ºC respectively; it is reasonable to assume that in most designs any valves and pumps in contact with these fuels would never rise above these temperatures. This means that a wide range of materials could be employed – and in particular coatings such as PTFE (operating temperatures up to 260 ºC) could be employed to prevent chemical interactions between fuels and hardware.

It may be useful to consider the construction of a Tektronix piezoelectric inkjet as shown in Figure 32. It is composed of a stack of photo-chemically machined, stainless steel plates brazed together at high temperature. The nozzle of diameter 80μm is shown enlarged on the right-hand side.

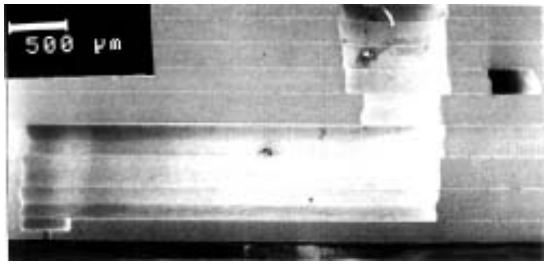

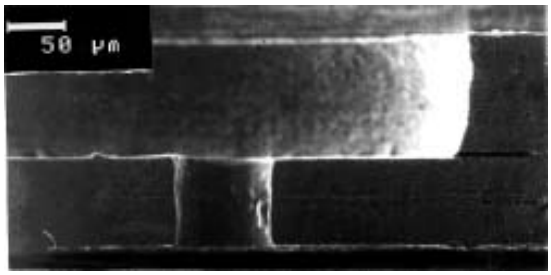

Figure 32 Tektronix piezoelectric inkjet, stainless steel stack (from Le Hue [1])

Micro-machined nozzles would need to withstand high temperatures. The main cause of heating of rocket injectors is caused by the recirculation of hot gases near the injector plate [33]. If droplet sizes were reduced, this would bring the combustion zone nearer to the injector plate and increase the temperature. Injector face plates are often made of a high conductivity material such as copper to re-distribute any such thermal stresses. Silicon has a thermal conductivity of 148W/(m-K) at 300K, comparable to brass and about half the value of copper.

Huzel [32] lists some materials that are known to be chemically unreactive with MMH and NTO fuels:

MMH	304,307 stainless steels , Aluminium, PTFE, Kel-F (PCTFE), polyethene
NTO	Aluminium, stainless steel, PTFE, Nickel alloy

It is likely that silicon would react with both these fuels, and need some form of protective coating. We suggest that Silicon Nitride, Oxide and Carbide be investigated for compatibility with fuels. Silicon Carbide is particularly attractive: it can be grown or deposited on a silicon substrate; it has excellent mechanical properties – hardness and wear resistance, and sublimes (rather than melts) at a temperature of 1800ºC ; it is not etched by most acids and can only be etched by alkaline hydroxide bases (i.e., KOH) at molten temperatures (600 C) [34]. Rajan [35] describes a SiC coated MEMS atomiser. The hardness of the SiC layer reduced the amount of wear and erosion seen on the corners of a comparable silicon design.

Stainless steel is also a strong candidate – it is chemically resistant, it can be combined with other micromachined materials, and small nozzles can be formed easily. Figure 33 shows a 50µm inkjet nozzle formed by electro-discharged machining (EDM).

EDM is also used to form the majority of nozzles for diesel injectors; it is often combined with Abrasive Flow Machining (AFM) to debur and produce specific exit radii.

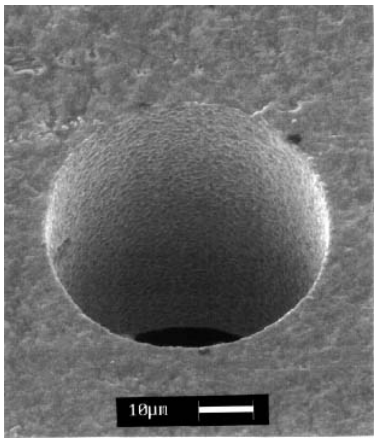

Figure 33 An SEM photograph of an EDM stainless steel nozzle (from Le Hue [1])

The blockage and fouling of nozzles is a significant concern as nozzle sizes are reduced. In early inkjets it was a common problem, and many current designs use disposable nozzles that are changed along with the ink-cartridge. Nabity [15] describes several measures used to reduce the problem when dealing with JP8 fuel:

> "Fouling could be caused by solid contaminant particles in the fuel, fuel tar residues left behind when the fuel evaporates, or by coke formation. First, there are commercially available filter systems that capture all particulates above 0.5 µm. We have used these types of filters successfully in our laboratory testing. Second, fouling due to tar condensation or fuel pyrolysis can be eliminated by pumping the fuel out of the injector during shutdown, thereby avoiding evaporation of stagnant fuel remaining in the flow passages. Third, under conditions expected at the nozzle, the majority of coke will form by one of two mechanisms: a catalytic mechanism that produces carbon filaments or a gas phase mechanism, which is referred to as condensation coke. [We] have developed methods to control each of these coke formation pathways."

Diesel injectors suffer from a steady build-up of deposits during their lifetime. A wide range of additives can be mixed with the fuel to reduce the problem. The problem should be less acute in a bipropellant rocket engine, as the combustion region does not normally touch the injectors.

9 Conclusions and Recommendations

Inkjets have been assessed as a possible method of injecting fuel into a bipropellant rocket engine. It was found that the surface tension effects that normally prevent unwanted ink escaping can only resist fuel pressures differences of the order of 0.05 bar for typical nozzle sizes. This means that unless the fuel pressure could be closely matched to the combustion chamber, and fluctuations in chamber pressure were much reduced there would be a need for valves. From considering the physics of devices it was found that the actuation technologies (piezoelectric, electrostatic; thermal-bubble consumes too much power) place limits on the maximum flow rates and blocking pressures of the inkjets. It was found that while inkjet are capable of suitable flow rates, none of the actuation technologies can also supply sufficient pressure. The only situation in which inkjets can generate sufficient pressure is if fuel pressure matched chamber pressure, and the chamber pressure fluctuations (from combustion instabilities) were reduced to less than 0.05 bar. The authors know of no actuation technologies under development that would change this situation in the foreseeable future. Additionally, during the intake part of the inkjets' cycle combustion chamber gases would be drawn into the inkjet body, with the risk of serious damage to the inkjet.

Diesel injectors for car engines were examined. The precise control over the injectors means that this type of technology offers the possibility of full throttling control, varying the mass flow rate (hence the thrust) from zero up to its maximum value, along with active control of combustion instabilities, and increased efficiency. The pressures found in diesel engines are very high (of order 1000 bar). Calculations show that at much lower pressures (e.g. 12 bar pressure difference for a 100μm nozzle) it would still be possible to atomise NTO and MMH fuels into droplets much smaller than nozzle diameters. A design concept has been proposed, along with some basic calculations to show its expected performance. Much further work is required to investigate this design fully.

The use of a membrane actuated atomizer has been investigated. This kind of injector will reduce the breakup length of about 4 times either allowing to reduce the combustion chamber length, hence saving mass, or increasing the combustion efficiency. No reduction should be expected in the droplet diameter if compared to a conventional injector. Experimental work is required to confirm the theoretical prediction and to effectively measure the droplet size and break up length.

Electrospray injectors has been studied. This kind of injection shows very attractive performance like no need of pressure drop along the injector plate, low power consumption,

extremely small droplet, active control on mass flow rate and droplet size hence the possibility of performing throttling control and active instabilities control. Unknown is the effects that the charged droplets will have on combustion and how this kind of injector will work with an applied pressure drop and if this will still be required to prevent the propagation of combustion instabilities upstream hence further theoretical and experimental work is required.

The following area have been identified as requiring further study:

(a) Both electrospray and active injectors have the potential to reduce droplet sizes. Study is required to determine the precise distribution of droplets that would be produced, and asses how this affects the combustion, in particular the dwell and mixing times of unburnt fuel, thermal modelling (the combustion may occur much closer to the injectors), and stability considerations.

(b) Active Injectors. A large program of study could be undertaken to develop a working prototype. Initially:

i. Injector design – detailed mechanical design, flow modelling, checking seating forces for low leakage.

ii. Reliability: How to isolate the actuators from chemically reactive fuels, thermal design, and consideration of clogging.

iii. Find and model an optimum configuration of injectors for efficient throttling and active control.

10 Acknowledgements

This project was funded by ESA through the Ariadna programme.

The authors wish to thank ESA, and in particular Cristina Bramanti for her help and assistance.

11 References

[1] P. Le Hue, "Progress and Trends in Ink-jet Printing Technology," *Journal of Imaging Science and Technology*, vol. 42, no. 1, pp. 49-62, 1998.

[2] J. K. Chen and K. D. Wise, "A high-resolution silicon monolithic nozzle array for inkjet printing," *IEEE Transactions on Electron Devices*, vol. 44, no. 9, pp. 1401-1409, Sept.1997.

[3] S. Kamisuki, T. Hagata, C. Tezuka, Y. Nose, M. Fujii, and M. Atobe, "A low power, small, electrostatically-driven commercial inkjet head," 1998.

[4] D. J. Laser and J. G. Santiago, "A review of micropumps," *Journal of Micromechanics and Microengineering*, vol. 14, no. 6, p. R35-R64, June2004.

[5] J. brunahl, "Physics of Piezoelectric Shear Mode Inkjet Actuators." Ph.D. Thesis Royal Institute of Technology, Stockholm, 2003.

[6] C. D. Meinhart and H. S. Zhang, "The flow structure inside a microfabricated inkjet printhead," *Journal of Microelectromechanical Systems*, vol. 9, no. 1, pp. 67-75, Mar.2000.

[7] F. M. White, *Fluid mechanics*, 3rd ed. New York: McGraw-Hill, 1994.

[8] J. Mueller, "Review and Applicability Assessment of MEMS-Based Microvalve Technologies for Microspacecraft Propulsion," in *Micropropulsion for small spacecraft*. M. Micci and A. Ketsdever, Eds. American Institute of Aeronautics and Astronautics, 2000, pp. 449-476.

[9] "EADS Bipropellant Thrusters and Apogee Motors," 2007. *online*: http://cs.space.eads.net/sp/SpacecraftPropulsion/BipropellantThrusters.html

[10] Morgan Electro Ceramics, *Piezoelectric Ceramics Properties and Applications* 2007.

[11] A. Olsson, G. Stemme, and E. Stemme, "A Valve-Less Planar Fluid Pump with 2 Pump Chambers," *Sensors and Actuators A-Physical*, vol. 47, no. 1-3, pp. 549-556, Mar.1995.

[12] M. T. Ahmadian and A. Mehrabian, "Design optimization by numerical characterization of fluid flow through the valveless diffuser micropumps,", 34 ed 2006, pp. 379-384.

[13] A. Olsson, P. Enoksson, G. Stemme, and E. Stemme, "Micromachined flat-walled valveless diffuser pumps," *Journal of Microelectromechanical Systems*, vol. 6, no. 2, pp. 161-166, June1997.

[14] M. Koch, "Silicon micromachined pumps employing piezoelectric membrane actuation for microfluidic systems." Ph.D. Thesis University of Southampton, 1997.

[15] J. Nabity and J. Daily, "A MEMS Fuel Atomizer for Advanced Engines," 2004.

[16] N. T. Nguyen, X. Y. Huang, and T. K. Chuan, "MEMS-micropumps: A review," *Journal of Fluids Engineering-Transactions of the Asme*, vol. 124, no. 2, pp. 384-392, June2002.

[17] P. Gravesen, J. Branebjerg, and O. S. Jensen, "Microfluidics-a review," *Journal of Micromechanics and Microengineering*, vol. 3, pp. 168-182, 1993.

[18] J. Nabity, S. Rooney, J. Daily, E. Johnson, and J. Hertzberg, "An Electrostatically Actuated MEMS Fuel Injector to Enhance Low-Pressure Atomization," 2006.

[19] G. D. Roy, S. M. Frolov, A. A. Borisov, and D. W. Netzer, "Pulse detonation propulsion: challenges, current status, and future perspective," *Progress in Energy and Combustion Science*, vol. 30, no. 6, pp. 545-672, 2004.

[20] SweetHaven Publishing Services, "Fundamentals of Gasoline and Diesel Fuel Systems," 2007. *online*: http://www.free-ed.net/sweethaven/MechTech/EngineMech/EngMech01_Main.asp

[21] Bosch, *Diesel-engine management*, 3rd ed ed. Stuttgart, Germany: Robert Bosch GmbH, 2004.

[22] S. W. Park, J. W. Kim, and C. S. Lee, "Effect of injector type on fuel-air mixture formation of high-speed diesel sprays," *Proceedings of the Institution of Mechanical Engineers Part D-Journal of Automobile Engineering*, vol. 220, no. D5, pp. 647-659, May2006.

[23] C. Bae, J. Yu, J. Kang, J. Kong, and K. Lee, "Effect of Nozzle Geometry on the Common-Rail Diesel Spray," *International Spring Fuels & LubricantsMeeting & Exhibition, Reno, Nevada* 2002.

[24] R. J. Santoro and W. E. Anderson, "Final Report on Combustion Instability Phenomena of Importance to Liquid Propellant Engines," Department of Mechanical Engineering and Propulsion Engineering Research Center, Pennsylvania State University,1994.

[25] A. H. Lefebvre, *Atomization and sprays*. New York: Hemisphere Publishing/Taylor & Francis, 1989.

[26] G. M. Faeth, L. P. Hsiang, and P. K. Wu, "Structure and breakup properties of sprays," *International Journal of Multiphase Flow*, vol. 21, pp. 99-127, Dec.1995.

[27] S. P. Lin and R. D. Reitz, "Drop and spray formation from a liquid jet," *Annual Review of Fluid Mechanics*, vol. 30, pp. 85-105, 1998.

[28] M. Archer and G. Bell, "Advanced Electronic Fuel Injection Systems - An Emissions Solution for both 2- and
4-stroke Small Vehicle Engines,"SAE 2001-01-0010, 2002.

[29] J. Whitehead, L. C. Pittenger, and N. J. Collela, "ASTRID Rocket Flight Test," *Energy and Technology Review*, vol. July 1994 1994.

[30] E. H. Yang, C. Lee, J. Mueller, and T. George, "Leak-tight piezoelectric microvalve for high-pressure gas micropropulsion," *Journal of Microelectromechanical Systems*, vol. 13, no. 5, pp. 799-807, Oct.2004.

[31] E. H. Yang, C. Lee, J. Mueller, and T. George, "Leak-tight piezoelectric microvalve for high-pressure gas micropropulsion," *Journal of Microelectromechanical Systems*, vol. 13, no. 5, pp. 799-807, Oct.2004.

[32] D. K. Huzel, H. Arbit, and D. H. Huang, *Modern engineering for design of liquid-propellant rocket engines*, Rev., updated and enl ed. Washington, DC: American Institute of Aeronautics and Astronautics, 1992.

[33] S. L. Bragg, "Rocket engines," 1962.

[34] M. Mehregany, C. A. Zorman, N. Rajan, and C. H. Wu, "Silicon carbide MEMS for harsh environments," *Proceedings of the Ieee*, vol. 86, no. 8, pp. 1594-1610, Aug.1998.

[35] N. Rajan, C. A. Zorman, M. Mehregany, R. DeAnna, and R. Harvey, "Performance of 3C-SiC thin films as protective coatings for silicon-micromachined atomizers," *Thin Solid Films*, vol. 315, no. 1-2, pp. 170-178, Mar.1998.

[36] B. Zuo, D.L. Black, D.S. Crocker, "*Fuel Atomization and Drop Breakup Models fro Advanced Combustion CFD Codes*", 38th AIAA/ASME/SAE/ASEE Joint Propulsion Conference & Exhibit, Indianapolis, July 2002.

[37] C. M. Waits, N. Jankowski, and B. Geil, "*Scalable Electrospray Components for Portable Power Application Using MEMS Fabrication Techniques*", Army Science Conference, Orlando, Florida, November 2006.

[38] D.C. Kyritsis, I.Guerrero-Arias, S. Roychoudhury and A. Gomez, "*Mesoscale Power Generation by a Catalytic Combustor using Electrosprayed Liquid Hydrocarbons*", Proceedings of the Combustion Institute, Volume 29, pp. 965–972, 2002.

[39] Deng, W., Klemic, J.F., Li, X., Reed, M.A., and Gomez,"*Increase of electrospray throughput using multiplexed microfabricated sources for the scalable generation of monodispersed droplets"*, Journal of Aerosol Science, **37**, pp. 696-714, 2006

[40] Deng, W., Waits, C.M., Jankowski, N., Geil, B. and Gomez, "*Optimization of Multiplexed Microfabricated Electrospray Sources to Increase the Flow Rate of Monodispersed Droplets*", 7th International Aerosol Conference, St. Paul, Minnesota,2006

Appendix A: Micropump data

The following table is based on data published by Laser [4] in 2004, and shows typical micropump performances from a wide range of research teams.

Author and year (see Laser [4] for references	Driver	Valves	Construction	Diaphragm material	Volume (mm3)	thickness (mm)	Voltage applied (V)	freq (Hz)	Pmax (kPa)	Qmax (ml min-1)	Qmax/Volume ((ml/min)l/min)
van Lintel 1988	Piezoelectric	Flap	glass-Si-glass	Glass	4100	0.3	125	0.1	24	0.0006	0.00015
Smits 1990	Piezoelectric	Peristaltic	glass-Si-glass	Glass	1500	n/r	100	15	5.9	0.1	0.0667
Kamper 1998	Piezoelectric	Flap	Molded	Brass/	500	0.15	n/r	70	200	0.4	0.8
Bohm 1999	Piezoelectric	Flap	Molded plastic	Brass	290	0.075	350	50	12	1.9	6.55
Gass 1994	Piezoelectric	Flap	glass-Si-glass	Glass	11800	0.3	250	40	9	0.55	0.0466
ThinXXS2000	Piezoelectric	Flap	Micro-injection	Plastic	4600	n/r	450	20	35	2.5	0.543
MIP Implantable	Piezoelectric	Flap	Glass-Si-Si-	Silicon	357	n/r	150	0.2	55	0.0017	0.00476
Esashi 1989	Piezoelectric	Flap	Siw/spun-Si-	Silicon	800	0.05	90	30	6.4	0.015	0.0188
Esashi 1989	Piezoelectric	Flap	Siw/spun-	Silicon	4000	0.05	100	25	10.7	0.018	0.0045
Li 2000	Piezoelectric	Flap	Si, glass	Silicon	3300	0.025	1200	3500	304	3	0.909
Carrozza 1995	Piezoelectric	Ball	Polymer-brass	Brass	1270	0.1	300	70	25	2.7	2.13
Stemme 1993	Piezoelectric	Nozzle / diffuser	Brass	Brass	2500	0.2	20	310	4.9	16	6.4
Gerlach 1995	Piezoelectric	Nozzle / diffuser	Si-Si-glass	Glass	200	0.12	50	3000	3.2	0.39	1.95
Olsson 1995	Piezoelectric	Nozzle / diffuser	Brass	Brass	1600	0.35	130	540	16	16	10
Olsson 1996	Piezoelectric	Nozzle / diffuser	Si-glass	Glass, silicon	270	0.3	n/r	1318	17	0.23	0.851
Bardell 1997	Piezoelectric	Nozzle / diffuser	Si-glass	Glass, silicon	220	0.5	290	3000	47	0.75	3.40
Olsson 1997	Piezoelectric	Nozzle / diffuser	Si-glass	Glass	260	0.5	200	3500	74	1.1	4.23
Schabmueller	Piezoelectric	Nozzle / diffuser	Si-Si	Silicon	120	0.07	190	2400	1	1.5	12.5
Zengerle 1995	Electrostatic	Flap	Si	Silicon	98	n/r	200	300	29	0.16	1.63
van de Pol 1990	Thermo-	Flap	Glass-Si-Si-	Silicon	3000	0.018	6	1	5.1	0.034	0.01133
Grosjean 1999	Thermo-	None	Acrylic,	Parylene/	970	0.12	n/r	2	3.4	0.0063	0.00649
Wego 2001	Thermo-	Flap	Printed circuit	Polyimide	780	0.0078	n/r	2	12	0.53	0.679
Yoon 2001	Thermo-	Flap	Si-glass	Silicone rubber	72	0.03	10	0.5	0.1	0.006	0.0833
Benard 1998	Shape-memory alloy	Flap	Silicon	TiNi	560	0.003	n/r	0.9	0.53	0.05	0.08932
Dario 1996	electromagnetic	Flap	Molded plastic	Rubber	2500	n/r	14	264	4.6	0.78	0.312
Bohm 1999	Electromagnetic	Flap	Molded plastic	Silicone rubber	1000	0.2	5	50	10	2.1	2.1